AD-A267 955

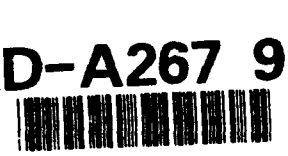

IMENTATION PAGE

Form Approved
OMB No. 0704-0188

...ENCY USE ONLY (Leave blank)	2. REPORT DATE	3. REPORT TYPE AND DATES COVERED
	June 1993	THESIS/DISSERTATION

4. TITLE AND SUBTITLE
An Investigation Into The Intergration Of Meter-Level Range And Millimeter-Level Phase Data Using A "Multimode Simulation For Optimal Filter Estimation" Software Package

5. FUNDING NUMBERS

6. AUTHOR(S)
Capt Sharyn Nancy McWhorter

7. PERFORMING ORGANIZATION NAME(S) AND ADDRESS(ES)
AFIT Student Attending: The Ohio State University

8. PERFORMING ORGANIZATION REPORT NUMBER
AFIT/CI/CIA- 93-115

9. SPONSORING/MONITORING AGENCY NAME(S) AND ADDRESS(ES)
DEPARTMENT OF THE AIR FORCE
AFIT/CI
2950 P STREET
WRIGHT-PATTERSON AFB OH 45433-7765

10. SPONSORING/MONITORING AGENCY REPORT NUMBER

11. SUPPLEMENTARY NOTES

12a. DISTRIBUTION/AVAILABILITY STATEMENT
Approved for Public Release IAW 190-1
Distribution Unlimited
MICHAEL M. BRICKER, SMSgt, USAF
Chief Administration

12b. DISTRIBUTION CODE

13. ABSTRACT *(Maximum 200 words)*

14. SUBJECT TERMS	15. NUMBER OF PAGES 126
	16. PRICE CODE

17. SECURITY CLASSIFICATION OF REPORT	18. SECURITY CLASSIFICATION OF THIS PAGE	19. SECURITY CLASSIFICATION OF ABSTRACT	20. LIMITATION OF ABSTRACT

DISCLAIMER NOTICE

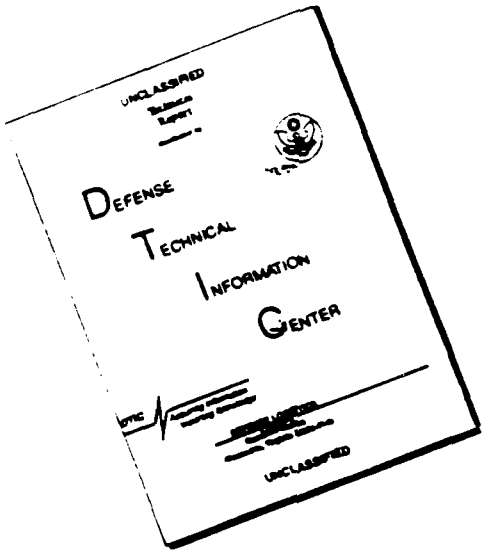

THIS DOCUMENT IS BEST QUALITY AVAILABLE. THE COPY FURNISHED TO DTIC CONTAINED A SIGNIFICANT NUMBER OF PAGES WHICH DO NOT REPRODUCE LEGIBLY.

AN INVESTIGATION INTO THE INTEGRATION OF METER-LEVEL RANGE AND MILLIMETER-LEVEL PHASE DATA USING A *"MULTIMODE SIMULATION FOR OPTIMAL FILTER ESTIMATION"* SOFTWARE PACKAGE

A Thesis

Presented in Partial Fulfillment of the Requirements for the
Degree Master of Science
in the Graduate School of The Ohio State University

by

Sharyn Nancy McWhorter, B.S. Physics, B.S.E.E.

* * * * *

The Ohio State University

1993

Master's Examination Committee:

Dr. Clyde C. Goad

Dr. Burkhard Schaffrin

Approved By

Clyde C Goad

Adviser
Department of Geodetic Science
and Surveying

To my husband, Russell,

with love

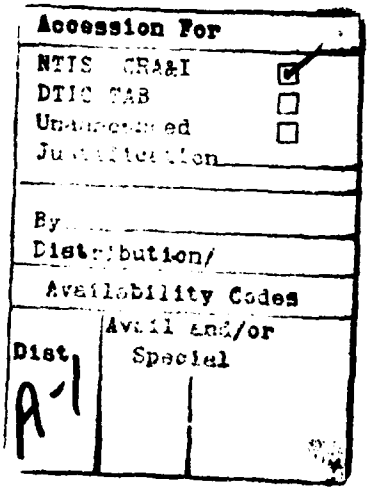

ACKNOWLEDGMENTS

In an undertaking such as this, many people contribute--both directly and indirectly. My case is no exception.

First, I will thank the faculty of The Department of Geodetic Science and Surveying. I stand in awe of them. Their combined knowledge is mind-boggling. They literally "wrote the book" in the field of Geodesy, and I am grateful for being a recipient of their decades of dedication to the profession. Geodesy has come a long way and continues to grow today. I am glad that I am now a part of it.

To the staff of the Department, thanks for all your support. Many thanks to Cindy Fowler for all her help getting around in the sometimes trying world of "modern technology." I really appreciated those vital pep talks from the viewpoint of someone who had been there before. Thanks, too, to Greta Sell for bearing with me and all my questions, requests, and phone calls.

My graduate advisor, Dr. Clyde Goad, deserves a special thank-you. His endless patience and guidance were more than generous. I enjoyed working with him and learning from his expertise in the field of GPS. I will take with me much more than his academic guidance provided. Although his much-deserved promotion to Department Chairman increased his workload tremendously, he still made time for me and all his other students. I am grateful for the many hours we struggled through the difficulties encountered in this thesis. Truly, I could not have finished this paper without his help.

Thanks must certainly go to Dr. Burkhard Schaffrin, as well. He opened my eyes in the field of Adjustment Computations and taught me how to see things from the "correct" perspective! I am grateful for his guidance during the writing of this paper.

Thanks also to my fellow students, especially Melita Kennedy and Dru Smith. We were all in the same boat, and through our combined efforts, we all managed to survive. My experience at The Ohio State University was a fruitful one in many ways, but being able to interface with students from over a dozen different countries was truly the most treasured experience. Despite our varied backgrounds, we found the common bond and bridged the gaps that geography often imposes on us.

I am very glad I had the opportunity to work along side of post-graduate students Dorota Grejner-Brzezinska, Dave Chadwell, Ming Yang, and Jarir Saleh. I learned so much from them and sincerely thank them for taking the time out of their busy studies to help me with mine. I wish them the very best of luck in their tough endeavors. I am confident that they will all be successful. I certainly will never forget how Dorota and I "must have done something wrong," even when we couldn't have!

To my parents and my sister I extend my love and my thanks for being there for me throughout my entire life. Thank you for always encouraging me and instilling in me the importance of experience, diversity, and the pursuit of happiness. Thank you also for telling me to never put a limit on my dreams.

By far, one person in my life outshines the rest. My undying love and most sincere thanks go to my husband, Russell. From my first day in graduate school to my last, he supported and encouraged me. He selflessly held things together when I was too busy to lend a hand. He kept me going when I didn't think I could. He knew I could succeed, even when I questioned my own abilities. We shared in the decision for me to attend graduate school, and now we share in this degree, just as we will continue to share in the wonders of life together.

VITA

14 September 1961	Born in Albuquerque, New Mexico
May 1979	Graduated from Sam Houston High School, Arlington, Texas
May 1983	B.S. in Physics, North Texas State University, Denton, Texas
22 June 1983	Received commission as an officer into the United States Air Force
May 1986	B.S. in Electrical Engineering, University of Missouri-Columbia
May 1986 to September 1991	Assigned to the Air Force Communications Command Operational Test and Evaluation Center, Wright-Patterson Air Force Base (AFB), Ohio
June 1993	M.S. in Geodesy, The Ohio State University, Columbus, Ohio
Future Plans	Follow-on assignment to Wright Laboratories, Wright-Patterson AFB OH

Field of Study

Major Field: Geodetic Science

TABLE OF CONTENTS

LIST OF TABLES

TABLE **PAGE**

LIST OF FIGURES

FIGURE **PAGE**

LIST OF ACRONYMS

AS	anti-spoofing
c	speed of light
C/A	Coarse/Acquisition
DOD	Department of Defense
DOP	Dilution of Precision
GPS	Global Positioning System
ICD	Interface Control Document
km	kilometer
m	meter
MHz	megahertz
mm	millimeter
msmt	measurement
MSOFE	Mulitmode Simulation for Optimal Filter Estimation
m/s	meter per second
ns	nanosecond
P-code	Precise Code
PRN	Pseudo-Random Noise
PPS	Precise Positioning Service

rms	root-mean-square
SA	selective availability
SPS	Standard Positioning Service
SV	Satellite Vehicle

CHAPTER 1

INTRODUCTION

1.1 Overview

This thesis is an investigation into the use of different types of Global Positioning System (GPS) data together with different types of bias sources. The intent was to examine their relative effect on the determination of the position of the receiver and the accuracy of the retrievable information. Selected inputs were processed through a simulation software package, "*Multimode Simulation for Optimal Filter Estimation (MSOFE)*" (Carlson and Musick, 1990). GPS users and researchers continually attempt to analyze the effects of data and measurement biases to increase the quality of information gained from the system. In this thesis, pseudorange and phase range data, together with various estimated and ignored measurement biases, were simulated and then processed through the optimal estimation software package. The output of the software--optimal estimations of the desired quantities--provided insight into the consequence of the virtually endless combinations of data.

1.2 Basic Statement of Problem

Figure 1 is a graphic representation of the underlying principle behind this thesis. What happens to our ability to recover positions when the most-simple, ideal situation is augmented with other forms of data and perturbed by biases?

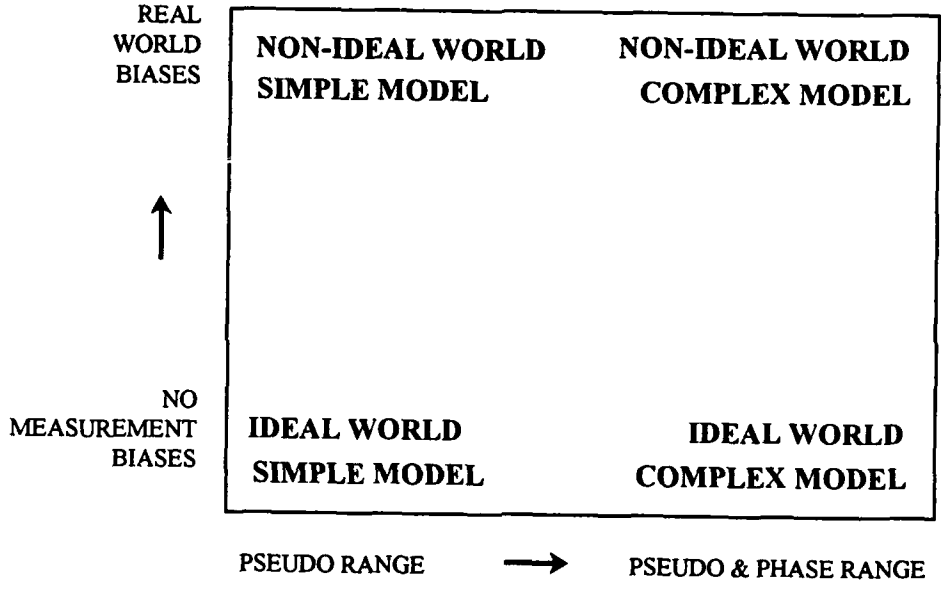

FIGURE 1

PRINCIPLE BEHIND THESIS

The preliminary stage utilized only the most basic GPS measurement type, the *pseudorange*, which is known to about one meter. The second stage, the incorporation of the *phase range*, known to about a millimeter, attempted to

increase the accuracy of the results. Minus any biases or errors, these combinations comprised the two "ideal" cases. To these ideal cases, perturbations in the form of biases[1] will be added piecemeal. The biases will fall into three different categories:

a. *station-dependent biases*--i.e., station coordinates in x, y, and z; and receiver clock biases[2];

b. *observation-dependent biases*--i.e., tropospheric delay, ionospheric delay, and phase integer ambiguity biases; and

c. *satellite-dependent biases*--i.e., satellite clock and radial orbit biases.

The study of adding additional data and biases will be accomplished with the MSOFE software package. This software provides for Kalman filtering--a sequential, recursive, mathematical data adjustment procedure designed to provide optimal estimation of errors within a linear system. Gelb (1992) describes an optimal estimator as that which is generated by

> a computational algorithm that processes measurements to deduce a minimum error estimate of the state of a system by utilizing: knowledge of system and measurement dynamics, assumed statistics of system noises and measurement errors, and initial condition information.

[1]In this thesis, the term "bias" will be used for those random effects on the measurement which must be modeled (systematically) and corrected for in order to obtain an accurate GPS range measurement (Wells, 1987).

[2]Although these quantities are typically estimated in a GPS adjustment, they are considered biases here because they influence the GPS measurement and must be accounted for as such.

Gelb further states that this form of estimation has some distinct advantages. First, the data processor (here, the computer program) is able to minimize the estimated error in a well-defined, statistical sense. Second, the processor is able to utilize all measurement data along with any *a priori* knowledge about the system (Gelb, 1992). This estimator is said to be used in a "filtering" capacity when the time at which the information is desired is the last available measurement epoch. That is, no future data are available for use in determining estimates at a desired epoch.

1.3 Research Approach

The basic approach to this research took many steps. First, attempts were made to learn the inputs and output of the MSOFE software. This program was actually the Kalman filter "shell" into which the proposed system designs had to be integrated. The filter design procedure began with the development of mathematical models to describe the actual physical system, the measurement system, the disturbance process, and the measurement error process (Musick, 1978). *In the strict context of the MSOFE program*, the program's documentation distinguishes between the "truth" and the "system" (Carlson and Musick, 1990) as follows:

> Truth: Defined as *all* real-world states related to the filter estimation process. This model is the starting point, from which less significant states are systematically eliminated in an effort to implement a more (computationally) practical system.

System: A subset of the "truth," defined by *all significant* real-world states affecting the filter estimation process. Included are the actual values of the filter states themselves plus higher-order measurement error states that significantly affect the filter states.

Within this software, the "truth" is deemed the full-order representation of the real world, the "filter" is the first-order representation, and the "system" is the second-order representation[3]. The program, MSOFE, requires adequate mathematical representation of both the "system" (also called the "system truth") and the "filter" models. The main focus in this thesis was to examine the effects on the "filter" performance due to higher-order error sources present in the "system truth" model (absent in the simplified "filter" model). The challenge was to develop a "filter" model that contained a sufficient number of states and sufficient measurement information to represent adequately the physical phenomenon of interest, here the GPS process and measurement models. Thus the model used for filtering was a much simpler model/subset of the system truth. Four station-dependent bias sources (the station coordinates x, y, and z; and the station clock) were maintained within the "filter" model. An addition of ambiguity unknowns was added when satellite phase data were also considered. The "system," which represented the real world, contained combinations of the three different bias types listed above.

[3]Here, the "real world" refers to the world as is seen from day to day--a state of being which is impossible to accurately model. Subsequently, the term "real world" will be used to define the model corrupted by biases (versus the "ideal world" with no biases). The distinction will be made again later for clarity.

The first step in writing software code to utilize the MSOFE program, once the details of the program were deciphered, was to develop the system model and the correct measurement model for the GPS pseudorange and phase range measurements. Recall that both the "system" and the "filter" models had to be distinguished between for MSOFE to appropriately estimate the desired quantities.

The incorporation of biases into the pseudorange and phase range measurement models was a step-wise procedure. The "filter's" state vector--the vector of estimated quantities--contained the four error sources inherent in any application of GPS: the station-dependent biases, listed above. Augmenting these basic four, biases were added to the "system truth" state vector to better represent the GPS case. First added were the observation-dependent biases and integer ambiguities.

Next, tropospheric delay models were added for phase and range measurements. The model for calculating the delay was taken from a currently used Hopfield model (Goad and Goodman, 1974). The delay caused by the ionosphere was next. Values for this bias source came from the model defined by the GPS receiver Interface Control Document (ICD), the model taking its inputs from the information within the broadcast ephemeris (Leick, 1990).

In an attempt to examine different measurement weightings, next was created a measurement noise model which depended on the elevation of the

satellite with respect to the station. Two different models were used: first, with the measurement noise dependent on the tropospheric delay of each satellite, and second, on the ionospheric delay of each satellite[4]. The models weighted each error source based on the satellite's elevation, the lower satellites contributing less weight than the higher ones. Based on the mathematical model, the four station-dependent unknowns required the presence of [at least] four satellites to estimate uniquely their values. However, only the addition of *redundant* satellites would affect the outcome using this elevation-dependent model. Results were expected to change only after the addition of a fifth satellite, because the weightings for the four-satellite case have no influence due to the lack of redundancy.

The next iteration explored the use of pseudorange and phase range measurements using an equal measurement uncertainty of ± 1 meter.

Next, the satellite-dependent biases were added to the model. Corresponding states in the state vector were (per satellite) two trigonometric coefficients and one satellite clock error term.

Finally, the issue of cycle slips was investigated by introducing a simulated cycle slip into the set of "filter" equations.

---

[4]Both tropospheric delay and ionospheric delay are functions of the satellite's elevation. These models will be called "elevation-dependent" models.

The measurement data and biases in this thesis were all simulated: each piece of information was *calculated* at each epoch. Attempts were made to derive measurement values that emulated actual observations as closely as possible. Input for calculating the data came from actual GPS broadcast ephemeris information and common error model schemes. The actual time tags "seen" by the broadcast ephemeris in generating orbit information were incremented in order to simulate the movement of the satellites during the test time. After every new iteration, the outputs of the filter were examined. Interest lay in the effects of these iterations on the position uncertainty of the station/receiver. Therefore, the results were presented in the form of graphs showing the receiver's position uncertainty versus time, where the uncertainty was presented as an *unscaled* dilution of precision (DOP) in meters[5]. The results from each iteration were compared to the ideal cases and similar combinations of biases. Details, results, and further information are presented in Chapter IV, Research and Conclusions.

[5]Actually, this uncertainty is the square root of the trace of the filter's *error estimation* covariance matrix (covariance of estimated-minus-true states). DOP's, as such, are in units of "meters per meter," and are defined as the square root of the trace of the filter's error estimation covariance *divided by the uncertainty of the measured variable*. Thus, here, the uncertainty was presented in meters.

CHAPTER II
THE EXTENDED KALMAN FILTER

2.1 Overview

This chapter is designed to provide a review of Kalman filtering definitions, techniques, and applications to this thesis topic. Some fundamental knowledge (by the reader) of Kalman filters is assumed. The Kalman filter theory, as it pertains to the software package employed in this thesis research, will also be addressed. If further details about the Kalman filter are desired, the reader may obtain helpful information in the textbooks by Brown (1983), Gelb (1992), and Maybeck (1979).

2.2 Introduction to the Kalman Filter

According to Maybeck (1979), a Kalman filter is an "optimal recursive data processing algorithm"[1] . The definition may be broken up into parts to help clarify it.

[1]The concise definition of a Kalman filter differs from book to book. Fundamentally, the Kalman filter must be thought of as a *concept* and not as a tangible item such as an algorithm. Maybeck's definition expounds upon this idea by implying that the algorithm is the means by which the concept is carried out.

a. "Optimal" implies that the filter can incorporate all information provided to it. It processes all available measurements to estimate the variables of interest to the developer. "Optimal" also means that errors are minimized, in some respect. According to Maybeck, the filter is able to utilize knowledge of system and measurement dynamics, statistical descriptions of any noises and biases, and initial conditions of the variables of interest (ibid).

b. "Recursive" implies that the filter algorithm does not require the storage of huge amounts of data. As the data are processed, the updates are made, and then the processed data are not needed for any subsequent updating. Information pertaining to the past data is maintained sequentially within the update process[2].

c. "Data processing algorithm" implies that the filtering procedure is realized through the incorporation of discrete-time measurement data, rather than continuous time inputs. The Kalman filter not-so-aptly shares its name with the type of "black box filter" known to the electrical engineer, but here, the filtering process is generated more typically by a computer

[2]Recursive adjustment of data is also called "sequential" adjustment, in which measurements are incorporated sequentially, as they become available. This method is in contrast to the "batch" adjustment, in which all available measurements are used together, processed all at the same time.

program. However, the main idea behind the two types of filters is the same--imperfect inputs are processed into outputs which are optimized, with respect to the model assumptions.

Figure 2 shows the typical application for a Kalman filter (Maybeck, 1979). A system is driven by control variables, which are affected by errors and/or biases. The difficulty in "solving" the problem at hand is that knowledge of the system inputs and outputs may be the only information the user has to determine

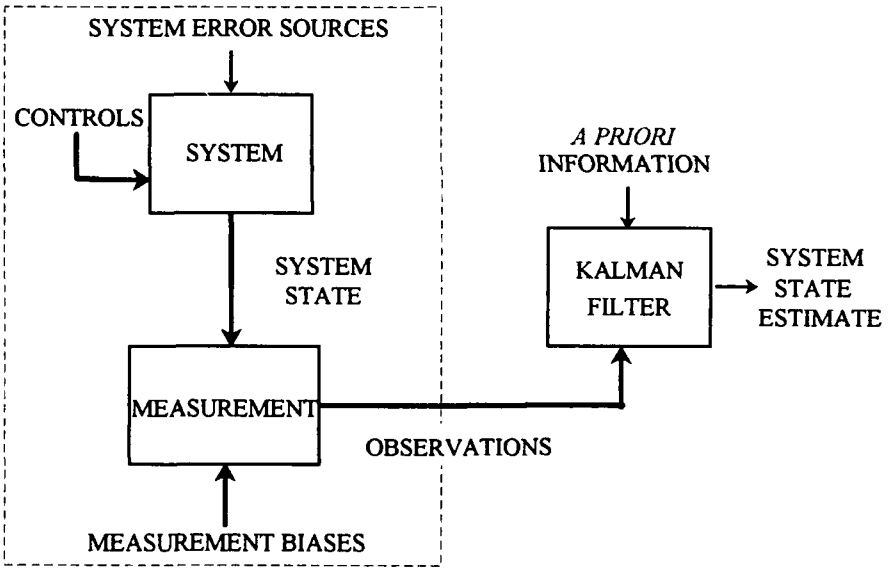

FIGURE 2

TYPICAL APPLICATION OF A KALMAN FILTER

the state of the system. The variables of interest will be called the system "states" and may or may not be directly measured. The measuring devices are the means for using collectible data to solve the problem of finding the estimates of the variables. Several different measuring devices may be available, as well. However, these measurement devices are also affected by error sources, usually in the form of biases and noises. The observations, together with the knowledge (current and prior) of the system and measurement devices, are combined in the Kalman filter. Prior knowledge may include the *a priori* knowledge of the system description and the measurement models. The output--the desired results--are optimal estimates of the variables of interest, more accurate than the estimates based on the individual measurements (Stacey, 1981).

The filtering process, as was indicated above, attempts to derive the optimal estimates from data obtained from the real world--a typically noisy and error-laden environment. The filter is designed to propagate the *conditional probability density* of the desired quantities, meaning the shape and location of the function depend on the measurements taken (Maybeck, 1979).

A further assumption with respect to the Kalman filter is that the system be described by a *linear* model, and the system and measurement noises are *white* and *Gaussian* (ibid)[3]. The "linear" requirement may be expanded to a non-linear system, provided the set of system equations is linearized about some nominal point or value

[3] These two requirements are necessary for the *maximum likelihood interpretation* of the optimal estimate to hold true.

not too far away (relatively) from the truth. This linearized model then becomes an error model, and filter process outputs will yield error estimations.

The "whiteness" of the noise means that the noise is not correlated in time--knowledge of the noise at any time, t, will not allow the user to predict the noise at time, $t+1$. The actual concept of the "whiteness" of noise is just an idealized means for visualizing the noise's "wideband" behavior in a "narrowband" system. "Gaussian," on the other hand, pertains to the amplitude of the probability density, taking on the shape of a bell-shaped curve, called the *normal probability density function*. The first- and second-order statistics of a noise process--namely the mean and variance--define the Gaussian density.

2.3 The Kalman Filter Models

Gelb (1992) states that before the filtering process can be successfully applied, proper *modeling* and *realistic performance projections* must be addressed. Three steps must be incorporated into the practical application of estimation theory:

a. design and computer evaluation of the "optimal" system behavior;
b. the design of suitable "suboptimal" system with cost constraints, sensitivity characteristics, computational requirements, measurement schedules, etc.; and

c. the construction of and test of a prototype system, making final adjustments or changes as warranted.

2.3.1 Basic Statistical Definitions

The *expectation* of a random variable, x, is defined as the sum of all values the random variables may take, where each value is weighted by the probability density with which the value is taken (ibid). Also called the *mean value* of x, the expectation of x is given by

$$E[x] = \int_{-\infty}^{+\infty} x\, f(x)\, dx \qquad (2\text{-}1)$$

where f(x) is the probability density function. In a probabilistic sense, the expectation is the value to which the average of a number of observations of x will tend to become as the number of observations increases.

The *mean squared value*, describing the distribution of x, is the expectation of x^2, written as

$$E[x^2] = \int_{-\infty}^{+\infty} x^2\, f(x)\, dx \qquad (2\text{-}2)$$

and the *root-mean-square* (rms) is the square root of the estimated $E[x^2]$. The *variance* (σ^2) of x is defined as the expectation of the deviation of the random variable from its mean (ibid):

$$\sigma^2 = \int_{-\infty}^{+\infty}(x - E[x])^2 f(x)dx \qquad (2\text{-}3)$$
$$= E[x^2] - E[x]^2$$

The square root of the variance is called the *standard deviation* of the random variable. One should note that the rms value and the standard deviation are comparable only for the zero-mean random variable.

The *covariance*, the measure of how the error in one random variable is related to the error in another, is the expectation of the product of the joint deviations from their respective means, written as:

$$E[(x - E[x])(y - E[y])] = \int_{-\infty}^{+\infty}\int_{-\infty}^{+\infty}(x - E[x])(y - E[y])\, f_2(x,y)\, dx\, dy$$
$$= E[xy] - E[x]E[y] \qquad (2\text{-}4)$$

where $f_2(x,y)$ is the *joint probability density function* of two random variables, x and y.

The *normal* probability density function, which characterizes the "Gaussian" process, is expressed as

$$f(x) = \frac{1}{\sigma\sqrt{2\pi}} \exp\left[-\frac{(x-\mu)^2}{2\sigma^2}\right] \qquad (2\text{-}5)$$

where μ is the mean and σ is the standard deviation of the random variable x. One may write the n-dimensional Gaussian vector $\underline{x}$ as in Equation 2-6[4].

$$\underline{x} \sim N(\underline{\mu}, \Sigma) \tag{2-6}$$

Equation 2-6 represents the standard notation for the random, Gaussian (normal) vector, $\underline{x}$, with mean $\underline{\mu}$ and covariance matrix Σ.

2.3.2 Kalman Equations

This section will outline the equations common to the Kalman filter mathematics and practical application. These equations are employed by MSOFE.

2.3.2.1 Transition Matrix

The dynamics of a continuous system may be represented by the first-order differential equation[5]

$$\dot{\underline{x}}(t) = \mathbf{F}(x(t),t)\,\underline{x}(t) + \mathbf{G}(x(t),t)\,\underline{w}(t) + \mathbf{L}(x(t),t)\,\underline{u}(t) \tag{2-7}$$

where $\underline{x}(t)$ = random state vector

$\underline{w}(t)$ = random forcing function

[4]The **boldface** notation indicates a matrix, while the underline notation indicates a vector.
[5]As all these vectors and matrices are time-dependent, the reference to time t will be dropped from subsequent equations, unless needed for clarity.

$\underline{u}(t)$ = deterministic (control) input vector

$\mathbf{F}(x(t),t)$ = homogeneous state dynamics matrix

$\mathbf{G}(x(t),t)$ = system process noise mapping matrix

$\mathbf{L}(x(t),t)$ = control input matrix.

Typically, the relation underlying Equation 2-7 is a non-linear ordinary differential equation, which must be linearized to be utilized in this context. This equation must be known together with stochastic prior information used in the linearization process, if Equation 2-7 is derived from a non-linear equation, in order for the process of Kalman filtering to hold (more about the linearization of this equation later). In this thesis, the GPS problem did not demand any controlling inputs, so the deterministic control term $\mathbf{L}\underline{u} = 0$, and Equation 2-7 for this case becomes

$$\dot{\underline{x}} = \mathbf{F}\underline{x} + \mathbf{G}\underline{w} \tag{2-8}$$

Further, the mapping matrix $\mathbf{G}$ is typically represented as the identity matrix $\mathbf{I}$, as dictated by the prior information used for linearization of the differential equation (if necessary). When $\mathbf{G} = \mathbf{I}$, the system noise remains unaltered (unscaled) as white. Such is the case here. Therefore, Equation 2-8 is written as

$$\dot{\underline{x}} = \mathbf{F}\underline{x} + \underline{w} \tag{2-9}$$

The differential equation given above must be sufficiently general such that any motion can be described through one of its solutions. If the state vector and forcing

functions in Equation 2-9 are defined at time t, then the states at any other time can then be predicted.

As an example, one may substitute into Equation 2-9 a particular dynamics matrix **D** for **F** and a particular white noise $\underline{w}'$ for $\underline{w}$ to get Equation 2-10.

$$\dot{\underline{x}} = \mathbf{D}\underline{x} + \underline{w}' \tag{2-10}$$

Descritizing Equation 2-10 and then through rearranging, one obtains:

$$\frac{\underline{x}_{t+1} - \underline{x}_t}{\Delta t} \approx \mathbf{D}\underline{x} + \underline{w}' \tag{2-11}$$

$$\underline{x}_{t+1} - \underline{x}_t \approx \mathbf{D}\underline{x}\,\Delta t + \underline{w}'\,\Delta t \tag{2-12}$$

$$\begin{aligned} \underline{x}_{t+1} &\approx \underline{x}_t + \mathbf{D}\underline{x}\,\Delta t + \underline{w}'\,\Delta t \\ &\approx (\mathbf{I} + \mathbf{D}\,\Delta t)\,\underline{x}_t + \underline{w}'\,\Delta t \end{aligned} \tag{2-13}$$

$$\Rightarrow \quad \underline{x}_{t+1} = \Phi(t+1,t)\;\underline{x}_t + \underline{u}_t \tag{2-14}$$

where $\underline{u}_t$ is the integrated noise vector and $\Phi(t+1,t)$ represents the *transition matrix*. The transition matrix is used for approximating the state vector at time t+1 by having prior knowledge of the state vector at time t. Equation 2-9 is actually the

equivalent to Equation 2-14; the former the *continuous* representation, and the latter the *discrete* representation[6].

2.3.2.2 Measurements

Gelb (1992) equates the importance of measurements to the *observability* of the system. According to Gelb, Gauss defines the observable system as one which possesses the number of observations that are absolutely required for the determination of the unknown quantities. The basic measurement equation may be seen in Equation 2-15.

$$\underline{z} = \mathbf{H}\,\underline{x} + \underline{v} \tag{2-15}$$

where $\underline{z} = \underline{z}(t)$ = the measurement vector

$\mathbf{H} = \mathbf{H}(x(t),t)$ = matrix that linearly relates $\underline{x}$ to $\underline{z}$ (observation matrix)

$\underline{v}$ = white measurement noise vector.

[6]The distinction between *continuous* and *discrete* must be made. Although the system process is a continuous one, the sampling of information (measurements, bias determinations, etc.) is conducted at specified, discrete time intervals (Brown, 1983). In this thesis, the sampling times are intentional and under the control of the programmer. As the system is considered continuous, the Kalman filter equations will be modeled for a continuous-time linear system with discrete measurements.

2.3.2.3 Errors

Recall Equation 2-9, assumed now to be a linear differential equation having been written in terms of the "whole value" state variables. However, the models employed in this thesis are non-linear and must be linearized, forming error models. Thus, the state vector written in terms of the error state variables, becomes

$$\delta \dot{\underline{x}} = \mathbf{F}\, \delta\, \underline{x} + \underline{w} \tag{2-16}$$

where $F_{ij} = \frac{\partial \dot{x}_i}{\partial x_j}$. Likewise, for the "whole value" measurement model, Equation 2-15, the measurement error model becomes

$$\delta\, \underline{z} = \mathbf{H}\, \delta\, \underline{x} + \underline{v} \tag{2-17}$$

where $H_{ij} = \frac{\partial z_i}{\partial x_j}$.

In Equation 2-18, one sees the representation of the error in the estimate vector (with the "tilde" ~) in terms of the estimated (with the "hat" $\wedge$) and the actual state value.

$$\tilde{\underline{e}}_x = \hat{\underline{x}} - \underline{x} \tag{2-18}$$

The covariance matrix Pof $\underline{\tilde{e}}_x$ will therefore be

$$P = E[\underline{\tilde{e}}_x \underline{\tilde{e}}_x^T] \tag{2-19}$$

assuming that $\underline{\hat{x}}$ is an unbiased estimate of $\underline{x}$. To cite a small example from Gelb (1992), given the error estimate as the two-state vector in Equation 2-20,

$$\underline{\tilde{e}}_x = \begin{bmatrix} \tilde{e}_1 \\ \tilde{e}_2 \end{bmatrix} \tag{2-20}$$

the covariance P will be (under the assumption that the expectation of each respective state is zero)

$$P = E\left\{\begin{bmatrix} \tilde{e}_1^2 & \tilde{e}_1\tilde{e}_2 \\ \tilde{e}_1\tilde{e}_2 & \tilde{e}_2^2 \end{bmatrix}\right\} = \begin{bmatrix} E[\tilde{e}_1^2] & E[\tilde{e}_1\tilde{e}_2] \\ E[\tilde{e}_1\tilde{e}_2] & E[\tilde{e}_2^2] \end{bmatrix} \tag{2-21}$$

An important item to note is that the square root of the trace of P is the rms length of the uncertainty of the estimated state vector $\underline{\hat{x}}$.

The covariance for the white noise forcing function $G\underline{w}$ is defined as (Gelb, 1992)

$$E[(G_t w_t)(G_\tau w_\tau)^T] = G_t Q_t G_t^T \delta(t-\tau) \tag{2-22}$$

where **Q** is the process noise strength matrix and δ is the Dirac delta function. Information for **Q** comes from the prior information used for the linearization of Equation 2-8. If one lets the process noise distribution matrix **G** be the identity matrix, Equation 2-22 becomes

$$E[w_t w_\tau^T] = Q_t \delta(t-\tau) \tag{2-23a}$$

$$\Rightarrow E[w(t_i)w(t_j)^T] = \begin{cases} Q & \text{for } t_i = t_j \\ 0 & \text{for } t_i \neq t_j \end{cases} \tag{2-23b}$$

which is now the covariance matrix of the white noise $\underline{w}$. One can also write that the mean of this white noise vector is

$$\mu_w = E[\underline{w}] = 0 \tag{2-24}$$

Likewise, for the white measurement noise vector $\underline{v}$, one can write that the mean is (Maybeck, 1979), assuming proper modeling in Equation 2-15,

$$\mu_v = E[\underline{v}] = 0 \tag{2-25}$$

and the covariance is

$$E[\underline{v}(t_i)\underline{v}(t_j)^T] = \begin{cases} R & \text{for } t_i = t_j \\ 0 & \text{for } t_i \neq t_j \end{cases} \tag{2-26}$$

One should also note that no correlations occur between $\underline{w}$ and $\underline{v}$, as seen in Equation 2-27.

$$E[\underline{w}(t_i)\underline{v}(t_j)] = 0 \tag{2-27}$$

2.3.2.4 Update Equations

The process of the Kalman filter is designed to "propagate" (by numerical integration) the error state vector and its covariance from the instant in time immediately following the most recent measurement update t_i^+ to the instant in time immediately preceding the next measurement update t_{i+1}^- (Stacey, 1991)[7]. The values for the state vector and covariance matrix at t_{i+1}^- are the predicted values from which the next updates are made (using the measurements). The following differential equations used in this integration are given (without proof) in Equation 2-28 and 2-29 (Maybeck, 1979).

$$\dot{\hat{\underline{x}}} = F\hat{\underline{x}} \tag{2-28}$$

$$\dot{\hat{P}} = F\hat{P} + \hat{P}F^T + GQG^T \tag{2-29}$$

at some time t_i with the initial conditions

[7]The notation "super -" indicates the condition prior to the measurement update (the predicted), and the "super +" indicates the condition after the update.

$$\hat{\underline{x}} = \hat{\underline{x}}(t_i^+)$$
$$\hat{P} = \hat{P}(t_i^+) \qquad (2\text{-}30)$$

as provided by the measurement cycle at time t_i.

After propagation, the estimates of $\underline{x}$ and **P** are updated, meaning that state estimates are revised based on new information (Stacey, 1991). Recall Equation 2-15 for the measurement model. One can write the updated state vector as

$$\underline{x}^+ = \underline{x}^- + K\Delta\underline{z} \qquad (2\text{-}31)$$

where $\Delta\underline{z}$ is the measurement residual and **K** represents the time-varying Kalman filter gain matrix, an integral element in the update equations (to be explained later). The measurement residual may be written in terms of the state prior to the measurement update ($\underline{x}^-$, thought of as the *predicted* state vector), changing Equation 2-31 to Equation 2-32:

$$\underline{x}^+ = \underline{x}^- + K(\underline{z} - H\underline{x}^-) \qquad (2\text{-}32)$$

Substituting in the measurement $\underline{z}$, written in terms of the actual state at the time t, Equation 2-32 becomes

$$\underline{x}^+ = \underline{x}^- + K[(H\underline{x} + \underline{v}) - H\underline{x}^-] \qquad (2\text{-}33)$$

By letting Equation 2-34 represent the error of the state based on the prior value of the state,

$$\delta\underline{x}^- = \underline{x}^- - \underline{x} \tag{2-34}$$

then Equation 2-33 may be written as

$$\underline{x}^+ = \underline{x}^- + K(-H\delta\underline{x}^- + \underline{v}) \tag{2-35}$$

Subtracting $\underline{x}$ from each side and defining

$$\delta\underline{x}^+ = \underline{x}^+ - \underline{x} \tag{2-36}$$

as the error of the state based on its updated value, one gets

$$\delta\underline{x}^+ = \delta\underline{x}^- + K(-H\delta\underline{x}^- + \underline{v}) \tag{2-37}$$

Rearranging Equation 2-37 gives the equation for the state error vector update:

$$\delta\underline{x}^+ = (I - KH)\delta\underline{x}^- + K\underline{v} \tag{2-38}$$

Then, the covariance of this updated state's error is

$$P^+ = (I - KH)P^-(I - KH)^T + KRK^T \tag{2-39}$$

where **R** is defined in equation 2-25 and P^- is the predicted covariance matrix prior to the measurement incorporation.

The Kalman gain matrix **K** should be discussed. This gain is a means for weighting new information as it becomes available to the system. This new added information can be thought of as causing the difference between the actual measurement and the filter's estimate of this measurement (Stacey, 1991). The Kalman gain matrix is designed to improve the estimate of the state vector by using information contributed by the observations. The gain matrix uses knowledge of measurement noise statistics and filter-computed covariances from previous epochs to make the updates. Without proof, the Kalman gain matrix for a continuous system/discrete observation model is (Gelb, 1992)

$$K = P^-(H^-)^T[H^-P^-(H^-)^T + R]^{-1} \tag{2-40}$$

where $H^- = H(\hat{\underline{x}}^-)$. This value of K is the precise value that minimizes the trace of the P^+ covariance matrix (*ibid*). Substituting Equation 2-40 into Equation 2-39, one gets the optimized value for the updated estimation error covariance matrix, seen in Equation 2-41.

$$P^+ = (I - KH)P^- \tag{2-41}$$

2.3.2.5 Updated Equations with Real-World Errors

The previous section described the update procedure when standard measurement models (with noise only) are used. However, in the real world, the measurement models and state equations should include biases due to real-world problems[8]. The more realistic measurement model may be written as

$$\underline{z} = \mathbf{H}\,\underline{x} - \mathbf{M}\underline{\gamma} + \underline{v} \tag{2-42}$$

where $\underline{\gamma}$ = the vector of additional random error states (here, called biases),

M = corresponding mapping matrix, and

the negative sign is used only as a convention.

The update of the state vector may now be written, as in Equation 2-31, as

$$\begin{aligned} \underline{x}^{+} &= \underline{x}^{-} + K(H\underline{x} - M\underline{\gamma} + \underline{v} - H\underline{x}^{-}) \\ &= \underline{x}^{-} + K(-H\delta\underline{x}^{-} - M\underline{\gamma} + \underline{v}) \end{aligned} \tag{2-43}$$

Following the same procedure as in Section 2.3.2.4, one can write the state error vector update equation as

$$\delta\underline{x}^{+} = (I - KH)\delta\underline{x}^{-} - KM\underline{\gamma} + K\underline{v} \tag{2-44}$$

---

[8]Recall the definition of "bias" here is not defined in the statistical sense, but implies a random influence on the GPS measurement which must be modeled (systematically) and accounted for.

and the covariance of this updated state's error is

$$P^{+} = (I - KH)P^{-}(I - KH)^{T} + KRK^{T} + KMP_{\gamma}M^{T}K^{T} \qquad (2\text{-}45)$$

where P_{γ} is the covariance of the error/bias (real-world) vector; $E[\gamma] = 0$; and no correlations exist between $\underline{\gamma}$ and $\underline{v}$ or $\underline{w}$, respectively.

One should note a very important point in Equation 2-45. The last term represents the addition to the state vector's uncertainty due to the presence of the unmodeled errors in the observation equations. MSOFE enables the user to look at both of the following[9]:

a. The output of the filter, i.e., *the filtering process's* estimate of the error it commits in estimating the entire filter state vector (represented by Equation 2-39); and

b. The "true" state vector estimation error, i.e., the "true" covariance of error in the filter-computed state as a random process driven by the true, real-world system state (represented by Equation 2-45).

Furthermore, one must assume here that the $\underline{\gamma}$ vector is a vector of "random biases" which affect the GPS measurement and does not contain quantities to be

[9]The distinction here is one strictly imposed by MSOFE. Recall that MSOFE distinguishes between the "system truth" (or equivalently "system") and the "filter" state vectors.

estimated by the filtering process. In turn, the covariance matrix, P_γ, will be considered *bounded*. This assumption will allow one to consider only defined covariances and ignore the unique situation when P_γ becomes unbounded (i.e., approaches infinity).

CHAPTER III
GLOBAL POSITIONING SYSTEM

3.1 Basic Theory

In this chapter, some of the basic concepts behind the Global Positioning System (GPS) will be summarized, beginning with a short background through to a summary of the measurement model employed in the research for this thesis. A moderate amount of information will be assumed already known by the reader. The topics represented here play a roll in the subsequent chapter dealing with the actual research. For further details about GPS theory, the reader may obtain helpful information from the textbooks by Leick (1990) or Wells (1987).

3.1.1 Background

The concept for the GPS is to serve the United States' military community. The United States Department of Defense (DOD) designed the system to be a military navigation system based on a world-wide coverage of a constellation of 24 satellites, or space vehicles (SV) (Stacey, 1991). The design for the satellites' orbit and earth coverage intended to provide 24-hour weather, navigation, timing, and surveying capabilities (Leick, 1990).

The designed constellation of satellites was originally to give the best possible coverage over the largest area of concern (in the military field, the two areas of concern were the southwestern continental United States and off the northeast coast of the United States in the North Atlantic Ocean). The satellites are positioned in orbits approximately 20,000 kilometers above the surface of the earth. The satellites have a orbital period around the earth of 12 sidereal hours. Due to the differences between the sidereal and solar time, the satellites appear almost 4 minutes earlier each day, the coverage advancing by approximately 30 minutes each week (Wells, 1987).

The average designed life span of each satellite ranges from 5 to 7.5 years. The satellites are equipped with solar panels which charge batteries during periods of sunlight. Some basic functions of the satellites are (ibid) :

(a) To receive and store information transmitted by the system operators;
(b) To conduct limited data processing using an on-board microprocessor;
(c) To maintain accurate time by means of several highly accurate oscillators;
(d) To transmit information to the user through propagated signals;
(e) To maneuver using thrusters controlled by the system operators.

Due the height of the orbit of the satellites, approximately three times the radius of the earth, any particular satellite may be visible to the user for approximately 5 hours each revolution. Based on the configuration, time of day, and location on the earth, the user may "see" 4 to 10 satellites above the horizon at any one time (ibid). However, due the geometry of the satellites with respect to the station (user), the

ability to recover positions will vary from time to time. In fact, the geometry of the satellites with respect to a receiver plays a major role in the user's ability to recover station position accurately. Think of the satellites in the sky and the receiver on the ground forming a polyhedron; the larger the volume of the polyhedron, the smaller the recovered position uncertainty (the ideal geometry or positioning of the satellites over the receiver places one satellite overhead and the other three on the horizon, 120 ° apart in azimuth. This geometry (ideally) allows for the best recovery of the receiver's position (ibid)). As the satellites move through the sky, this geometry will change, as will the volume of the "polyhedron" and the recovered position uncertainty.

3.1.2 Signal Structure

The fundamental frequency for transmission of information by the satellites is defined as f_o = 10.23 MHz. Each satellite transmits two carriers at two different frequencies:

$$L_1 = 154\ f_o = 1575.42\ \text{MHz} \qquad (3\text{-}1)$$

$$L_2 = 120\ f_o = 1227.60\ \text{MHz} \qquad (3\text{-}2)$$

The L_1 is modulated with two types of code (P-code and C/A-code), and the L_2 is modulated with only one type of code (P-code); both contain the navigation message.

The codes are called pseudo-random noise (PRN) codes and consist of a series of +1's and -1's emitted at particular frequencies. If the code value is -1, the carrier

phase is shifted by 180°; if the code is +1, the carrier is unchanged. The phase shift of the signal may be seen in the following picture, indicated by the arrow in Figure 3.

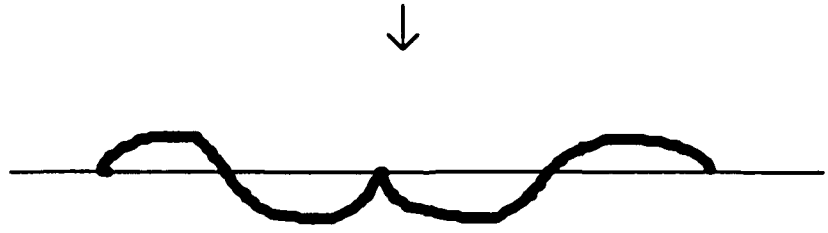

FIGURE 3

REPRESENTATION OF PHASE SHIFT OF CARRIER PHASE

The C/A-code (or coarse/acquisition code, also more recently called Standard Positioning Service (SPS)) is the code available to the civilian community. The C/A-code is a relatively short code of 1023 bits, with a duration of 1 millisecond (msec) and an emission (chipping) rate of 1.023 Mbps (megabits per second) (Spilker, 1980). The chipping rate may be thought of as the rate at which the phase is shifted, the means for determining the beginning of a piece of data (e.g., the navigation message). Each satellite transmits mutually exclusive C/A codes, making it possible to distinguish signals received simultaneously from the satellites (Leick, 1990). The C/A-code is only available on the L_1 carrier.

Considering the speed of light, $c \approx 3 \times 10^8$ m/s, the length of the C/A signal is approximately 300 meters. One can expect the uncertainty in position associated with this code to be approximately 1% of the code length, or ≈ 3 meters (ibid).

The P-code (or precise code, also more recently called Precise Positioning Service (PPS)) emits signals at 10.23 Mbps, repeating itself every 37 weeks (267 days). This code is initialized at the beginning of each week (the "GPS week" is defined as the time from midnight Saturday to Sunday (ibid)), but is not mutually exclusive as is C/A code. However, each satellite is assigned its own weekly portion of the code, and some weeks will not be utilized, because there are less than 37 satellites in the GPS. The P-code is available on both the L_1 and the L_2 carriers. With an approximate code length of 30 meters, the uncertainty of the position recovery is $\approx$ 0.3 meters = 30 centimeters.

A third type of code, the Y-code, is similar to the P-code, but is classified by the DOD and is usable only to those users who have access to the encryption key. The intent of this type of code is to provide a secure code to which other users cannot deny its access. This method of selectively providing access to users is called *anti-spoofing* (AS)[1].

Both carrier frequencies transmit the navigation message. This message is a 50-Hz stream of data designed to notify the user of the position and other pertinent information about the satellite. The message contains information on the ephemerides of the satellites, the GPS time, the behavior of the clock, and any system status messages.

[1] This type of code will not be addressed further in this thesis, but is mentioned only as background information.

The DOD has chosen to maintain controls on the users of the GPS by a method called *selective availability* (SA). When desired, the Master Control Station (the central location for updating broadcast and satellite orbit information) located in Colorado Springs, Colorado, will transmit degraded information. The broadcast information may include "orbit perturbations" which will lead to degraded ephemerides. The atomic clock times may also be perturbed (dithered)[2].

3.1.3 Pseudorange

The first and most common type of measurement which can be made by the GPS receiver is the *pseudorange*. In the simplest terms, the *range* is the distance between the satellite and station (receiver). As this measurement is impossible to explicitly measure with ordinary measuring devices (due to the motion of the satellites and the possible motion of the receiver), the GPS receiver uses the timing of signals to arrive at the satellite-station distance. The time the signal takes to travel from satellite to station is given by

$$\Delta t = t_R - t^S , \tag{3-3}$$

where the "R" and "S" denote "receiver" and "satellite," respectively. Its equivalent "distance" would be $c\Delta t$, where c is the speed of light. This value would be the exact range if neither the clock in the satellite nor the clock in the receiver were in error. Alas, this exactness does not exist in the real world. We expect both clocks to be in

[2]Selective availability serves to degrade instantaneous, real-time position calculations, but post-processing methods could allow a more accurate determination of positions.

error by some amount, so neither clock contains the correct time. The measured time, t, on either the satellite clock or receiver clock can be given by

$$t = t^* + \delta t \tag{3-4}$$

where t^* = the correct (true) time, without errors, and

δt = the correction necessary due to the inaccuracies in the clocks.

Therefore, the actual range measured by the GPS receiver, barring any other error sources or biases and using the definition for range above, will be

$$R = ct_R - ct^S \tag{3-5}$$

$$\begin{aligned} \Rightarrow R &= c(t_R^* + \delta t_R) - c(t^{S^*} + \delta t^S) \\ &= c(t_R^* - t^{S^*}) + c\delta t_R - c\delta t^S \\ &= \rho + c\delta t_R - c\delta t^S \end{aligned} \tag{3-6}$$

with ρ representing the true geometric distance between satellite and receiver. The value, R, is called the *pseudorange* because of the presence of clock errors and their addition into the calculation of the range. To be more precise, Wells (1987) defines the pseudorange as the

> time shift required to line up a replica of the code generated in the receiver with the received code from the satellite multiplied by the speed of light

where the "time shift" is the difference between the time of the received signal and the emitted signal, measured in the receiver's and the satellite's time frames, respectively. The navigation message from each satellite contains the necessary information for the evaluation of the satellite clock offset, δt^S, in Equation 3-6.

The distance could also be found by calculating the length of the vector from satellite to receiver in Equation 3-7,

$$\rho_R^S = \sqrt{(x^S - x_R) + (y^S - y_R) + (z^S - z_R)}, \qquad (3\text{-}7)$$

where ρ_R^S = range from satellite, S, at epoch t^S to receiver, R at epoch t_R; and

x, y, z (normally) denote the earth-centered, earth-fixed coordinates of the satellite and receiver. Therefore, including clock errors, the pseudorange becomes:

$$R_R^S = \rho_R^S + c\delta t_R - c\delta t^S + \varepsilon_R^S \qquad (3\text{-}8)$$

where ρ_R^S is found using Equation 3-7,

$c\delta t_R - c\delta t^S$ is the clock correction term from Equation 3-6, and

ε_R^S is the noise term.

3.1.4 Phase Range

The second type of measurement we can extract from a GPS receiver is the *phase*. According to Wells (1987), the carrier beat phase is "the phase of the signal which remains when the incoming Doppler-shifted carrier is differenced (beat) with

the constant frequency generated in the receiver." In simple terms, the phase is the number of cycles the carrier travels from satellite to receiver[3]. The *phase range* is therefore the phase converted to an equivalent distance in meters (by multiplying by the wavelength of the signal). Here, phase range measurements will be used. Just as with the pseudorange, the phase range is impossible to measure explicitly. The equation for the phase range measured by the receiver is

$$\varphi_R^S(t_R) = \varphi^S(t_T) - \varphi_R(t_R) \tag{3-9}$$

where t_R = the time at the receiver, and

t_T = the time at the transmitter = $t_R - \rho/c$ where ρ = the distance traveled in a vacuum and c = the speed of light.

This equation for phase ranges differs from that of pseudoranges because the latter uses the differences between times, and the former differences phase range values at the satellite and receiver. The phase is made up of a whole number of wavelengths between satellite and receiver plus the fraction of wavelength remaining. It is this fraction which is actually measured by the receiver; the whole number (integer) is the more difficult value to determine. Therefore, one may think of the phase range as (without the presence of any other biases)

$$\varphi_R^S(t_R) = \varphi^S(t_T) - \varphi_R(t_R) - \rho_R^S \tag{3-10}$$

[3]However, this is not what is measured on the GPS receiver. This will be explained later.

where the first two terms represent the non-synchronicity of the two clocks expressed in wavelengths, and ρ_R^s is the geometric range from Equation 3-7. If the clocks were perfectly aligned, the measured phase range would exactly equal the geometric range (barring the presence of any other biases or errors).

Recall the values for the frequencies of the carrier and the two codes. The carrier wavelength is much shorter than either of the codes' wavelengths. Using the same logic used above for pseudoranges, one can expect the precision of the phase ranges to be much better (higher) than that of the pseudoranges. For the L_1 carrier, the wavelength is approximately 19 cm. Using the typical value of 1%, the phase measurements can be made to approximately 1% of the wavelength, or approximately 0.2 cm = 2 mm. As good as this appears on the surface to the potential users, special problems plague the phase measurement technique, as will be mentioned a bit later.

3.2 Measurement Biases

Because the real world is continually plagued with imperfections, the measurements attained from the typical GPS receiver will not be representations of the exact range between satellite and receiver. Three types of biases[4] will be covered in this thesis:

[4]Recall that this thesis defines the "bias" as any random effect on the GPS measurement which must be (systematically) modeled and correct for in order to obtain an accurate range measurement. This definition may conflict with others' notation for the "bias" as a non-random quantity. The reader must keep these differences in notation in mind.

a. Station-dependent biases,

b. Observation-dependent biases,

c. Satellite-dependent biases.

3.2.1 Station-Dependent Biases

As was mentioned above in Section 3.1.3, the receiver clocks contain some error. One must account for this error to ensure the clock's bias does not affect the range values. Similarly, the data file taken from the receiver gives only *preliminary* information about the coordinates of the station; these coordinates are just approximations. In fact, these four values (station clock and the three station coordinates) are frequently the desired quantities to be extracted from a series of data.

3.2.2 Observation-Dependent Biases

Three observation-dependent biases exist which cause much consternation in the GPS community: tropospheric delay, ionospheric delay, and carrier phase integer ambiguity. All three types will be addressed in this thesis. The first and second types exist because of the presence of the GPS signal's propagation media.

3.2.2.1 Propagation Media

Electromagnetic radiation, regardless of its source, is affected by the propagation medium. Based on the governing laws of rays through a medium, the rays, in this case the satellites' signals, are said to refract due to the presence of the

medium. This bending is accompanied by a delay in the travel time of the rays. The bending action, per se, does not effect the GPS community as much as the time delay in the signals. The presence of the media physically lengthens the true path of the signal with respect the geometric distance from the satellite to the receiver, seen in Figure 4 (Goad and Goodman, 1974). The lengthened path means the signal has taken a longer amount of time to reach the satellite than would have been taken in a vacuum. This time delay biases the GPS measurements and must be modeled to remove, or at least suppress, the effects.

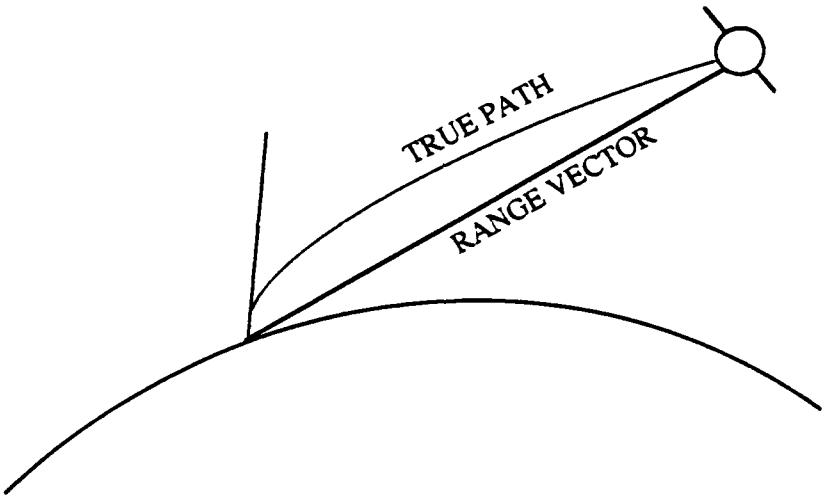

FIGURE 4

RANGE VECTOR VERSUS TRUE PATH

Effect of Propagation Media on GPS Signals

The propagation media for a typical GPS signal are the *troposphere* and the *ionosphere*. The troposphere is the portion of the atmosphere extending from the

earth's surface to about 40 km. The ionosphere extends from approximately 50 km to 1000 km in altitude (Wells, 1987). The two media's effects on the GPS signals are quite different, as are the means for modeling them. Both will be discussed here.

3.2.2.1.1 Troposphere

For frequencies below 30 MHz, the troposphere is said to behave as a *nondispersive* medium. A nondispersive medium is one in which the refraction of the signal is independent of the frequency of the signals being transmitted through it (Leick, 1990). This delay is very dependent on the pressure, temperature, and humidity of the medium (ibid). Because the true path is lengthened (the transmission time of the signal has increased), any correction due to the bias must be *subtracted* from the observed GPS measurement (pseudorange or phase range).

The troposphere, as in any atmospheric medium, is made up of a *dry* and a *wet* part. Both parts are modeled to predict the medium's effect on the signal. The dry portion of the troposphere makes up about 90% of the total refractive effect. This portion is commonly estimated using surface pressure and temperature data and is known to an accuracy of about 2% (Goad and Goodman, 1974).

The wet portion, although only 10% of the total refractive effect, is much more difficult to model. This portion is dependent on the conditions along the transmission path of the signal, often independent of the surface conditions. The model must include information about the water content of the atmosphere, the temperature, the altitude, and the elevation angle of the signal--some of which are very difficult to

model. The major problem with the modeling of the wet part lies in having accurate knowledge of the water vapor content. Localized water "pockets" in the atmosphere along with atmospheric turbulence create more problems in the modeling of the wet contribution. Various models exist which model this component, taking all the above difficulties into account.

The overall model for the contribution of the troposphere to the GPS signal is a combination of the wet and dry parts. Based on the information found in three different studies[5], the average correction for the troposphere based on the satellite's elevation with respect to the station may be found in Table 1 (ibid).

TABLE 1

AVERAGE TROPOSPHERIC CORRECTION

Based on Elevation Angle

Elevation Angle (degrees)	Average Correction (meters)
90	2.40
45	3.39
30	4.78
20	6.95
10	13.34
7.5	17.34
5	24.52
2	45.61
0	88.28

[5]The three studies referred to are those of Saastamoinen, Saastamoinen/Marini, and Hopfield. Complete references may be found in Goad and Goodman (1990).

3.2.2.1.2 Ionosphere

In the earth's ionosphere, the sun affects a fraction of the gas molecules by ionizing them with ultra-violet radiation, causing the release of free electrons. Just as with any electromagnetic signal propagating through an ionized medium, the GPS signals are affected by the non-linear *dispersive* characteristics of the medium. Unlike the nondispersive characteristic of the troposphere, the ionosphere *is* frequency-dependent, and the modulations on the carrier and the carrier phases are affected differently.

The dispersive effects of the ionosphere may be visualized by examining the dispersion curve in Figure 5 (Wells, 1987).

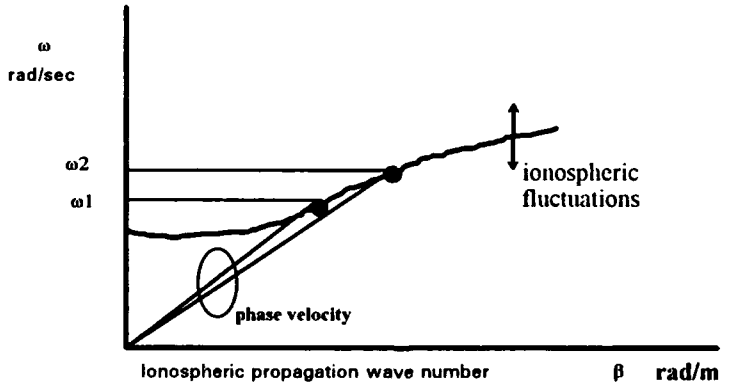

FIGURE 5

IONOSPHERIC DISPERSION EFFECTS OF THE MEDIUM

Ionospheric Propagation Wave Number vs. Angular Frequency

At any point in the curve, the slope of the line joining the origin to that point is the *phase velocity*, $v_p = \omega/\beta$, where $\omega = 2\pi f$ is the angular frequency of the signal in the ionosphere, and $\beta = 2\pi/\lambda$ is the ionosphere propagation wave number. The *group velocity*, $v_g = \partial\omega/\partial\beta$, is found by the local tangent slope at the point. The corresponding indices of refraction are

$$n_p = v_p/c \qquad \text{and} \qquad n_g = v_g/c \tag{3-11}$$

where c = speed of light in the vacuum. The respective indices of refraction for the ionosphere are (in a first-order approximation)

$$n_p \approx 1 - \frac{aN}{f^2} \qquad \text{and} \qquad n_g \approx 1 + \frac{aN}{f^2} \tag{3-12}$$

where N = ionospheric electron density in electrons/m^3 at the time and place of evaluation and a = constant (Wells, 1987). The change in path length due to the ionosphere is given by

$$\Delta\rho = \int (n-1)\, ds \tag{3-13}$$

which represents the integration along the propagation path. The GPS signals are dependent on the group index of refraction, so the ionospheric group delay is

$$\Delta\rho_g = +\frac{aN_T}{f^2} \qquad (3\text{-}14a)$$

The effect on the phase measurements is opposite in sign to the range effect seen in Equation 3-14a; the ionospheric phase delay, is, therefore,

$$\Delta\rho_p = -\frac{aN_T}{f^2} \qquad (3\text{-}14b)$$

where N_T in both equations is the total electron content along the propagation path in electrons/m^2.

The ionospheric effect also sees daily variations, the minimum between midnight and early morning, and the maximum around local noon, dependent on the activity of the sun (Leick, 1990). Depending on these factors, the total ionospheric effect could range from centimeters to tens of meters (Wells, 1987).

To reiterate, the most important effects of the ionosphere on the GPS signal are (Leick, 1990)

a. the retardation of the modulation on the carrier wave (i.e., the ionospheric time delay), causing an increase in the apparent path of the signal (pseudorange); and
b. the advancement of the carrier phase, causing a decrease in the apparent phase of the signal (phase range).

3.2.2.2 Carrier Phase Integer Ambiguity

When the GPS receiver is first turned on to take measurements, the cycle counter will read some arbitrary initial integer value. If the satellite's signal is *continually* received by the station during the measurement period (i.e., no "loss of lock" occurs to disrupt the flow of information from satellite to receiver), this integer will not change. Think of the phase range measurement Equation 3-10 as now possessing an ambiguity bias, shown in Equation 3-15,

$$\varphi_R^S(t_R) = \varphi^S(t_T) - \varphi_R(t_R) - \rho_R^S + N\lambda \qquad (3\text{-}15)$$

where $N\lambda$ is the integer times the wavelength of the carrier. If the world were ideal, the clocks would be synchronous, and the two quantities $[\varphi^S(t_T) - \varphi_R(t_R)]$ and φ_R^S (the reading on the GPS receiver) would equal zero. The geometric distance, therefore, would exactly equal the integer ambiguity, $N\lambda$. The term, $N\lambda$, represents the integer number of counts between the satellite clock and receiver clock. However, the receiver measures the fractional portion of the signal; only this fractional part is meaningful to the GPS user.

Actually determining the integer ambiguity value can be very difficult, if not impossible. It is difficult to locate the exact cycle of the carrier whose phase is being measured (Wells, 1974). Although not meaningful, this integer value must be resolved to properly process phase data. One way to eliminate its contribution is to difference two measurements which have the same ambiguity value, possibly at consecutive epochs, canceling out the ambiguity from the problem, altogether.

3.2.3 Satellite-Dependent Biases

Two types of satellite-dependent biases exist: orbit representation biases and satellite clock biases. Clock errors are present due to biases in the models for the clocks in the broadcast message (e.g., it is impossible for the clocks to be perfectly aligned to GPS time). Orbit biases exist because of the errors inherent in the satellite ephemeris information (e.g., the satellite is not where the broadcast message indicates that it is). Errors in the ephemeris may be eliminated by access to better orbit information. The GPS user is not often lucky enough to receive the most accurate information, and as such, must compensate for these biases. Forces not under the user's control continually act on the satellites, rendering what information the user does have as inaccurate. These forces are also very difficult to measure from *any* location on the earth's surface.

Orbital biases may naturally be expressed in the form of *radial*, *along track*, or *out of plane*, as seen in Figure 6. Using orbital data provided by the broadcast ephemeris, satellite positions can expect a typical accuracy of about 10-20 meters (Wells, 1987).

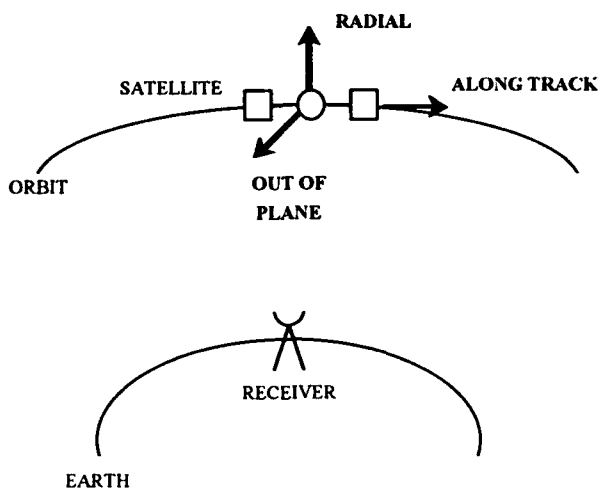

FIGURE 6

ORBITAL BIASES

Here, the orbital bias introduced into the measurement models will be a combination of the three different types. The combined bias may be thought of a periodic oscillation of the satellite along its orbit. These oscillations are fractions of the sine and cosine of the angular position of the satellite as a function of time, defined by the satellite's Keplerian elements, as in Equation 3-16. The value for Δr indicates the change in the radius of the orbit based on the trigonometric oscillations of the satellite.

$$\Delta r = S \sin \phi + C \cos \phi \qquad (3\text{-}16)$$

where ϕ = argument of perigee (ω) + true anomaly (f)

S and C = coefficients

The argument of perigee and the true anomaly place the satellite in the orbital plane at a particular epoch, as seen in Figure 7.

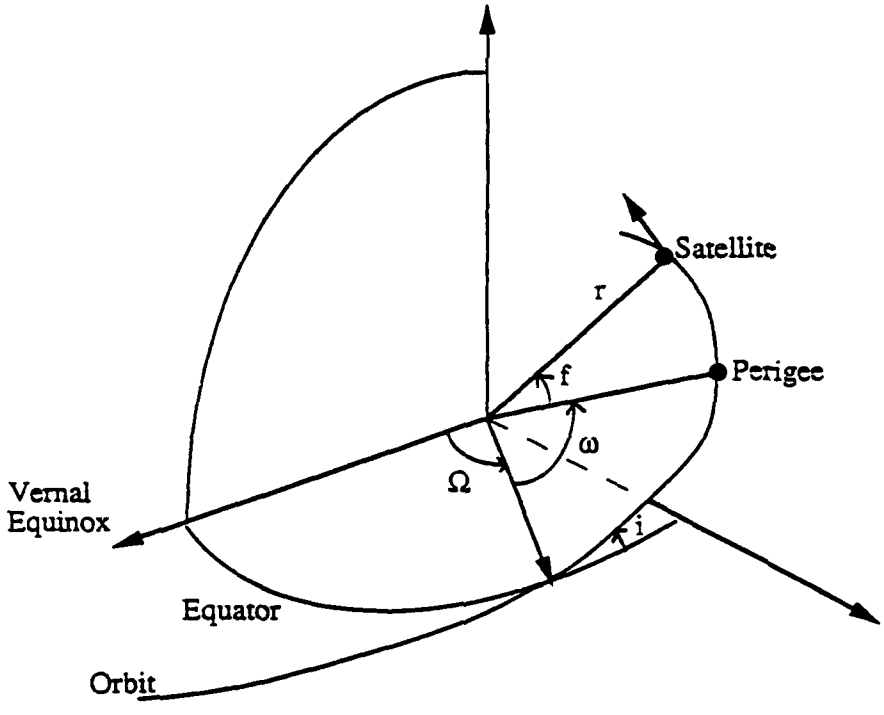

FIGURE 7

PLACEMENT OF THE SATELLITE IN THE ORBITAL PLANE

As Defined by the Keplerian Elements

3.3 Models

Each of these biases will be incorporated into the measurement model for use in this research. Biases often affect the pseudorange and phase range measurement differently, as will be shown below.

Recall that this thesis is a simulation of measurements and biases. The initial, imperfect values of the desired quantity will be termed the "nominal" value. Typically, corrections are applied to the nominal value to reach the "true" value. In Equation 3-17, the relationship between these three quantities is shown.

$$\text{truth} = \text{nominal} + \text{correction} \tag{3-17}$$

This *nominal* value is the value inserted into the measurement models, based on the theory of MSOFE and its unique requirements for setting up the problem at hand. Therefore, in all cases, the desired value will be corrected as

$$\text{desired (nominal)} = \text{truth} - \text{correction (true correction)} \tag{3-18}$$

where the correction will be the entry in the state vector, as applicable. As the person setting up the simulation, I shall supply the "truth" from which the nominal is found. The [best estimate of the] correction will be the output of the filter.

3.3.1 Model for Pseudorange Measurements

The final model for the pseudorange (in linear units) is given by Equation 3-19,

$$PR = \rho^* + c(t_R^* - t^S) + T^* + \frac{cI^*}{f^2} + S^* \sin\phi + C^* \cos\phi + c\Delta t^{S^*} + \varepsilon_{\substack{pseudo \\ range}} \qquad (3\text{-}19)$$

where

$\rho^* = \sqrt{[x^S - (x_R - \delta x_R)]^2 + [y^S - (y_R - \delta y_R)]^2 + [z^S - (z_R - \delta z_R)]^2}$

= geometric distance between satellite at t^S and receiver at t_R

$c(t_R^* - t^S)$ = speed of light * clock differences due to clock inaccuracies

where $t_R^* = t_R - \delta t_R$

T^* = tropospheric correction from Hopfield model = $T - \delta T$

cI^*/f^2 = speed of light * ionospheric correction, scaled by the square of the frequency of the carrier (in MSOFE, nominal = c(I - δI))

S^* = arbitrary coefficient of the sine term = S - δS

C^* = arbitrary coefficient of the cosine term = C - δC

ϕ = location of the satellite in the orbital plane based on Keplerian elements

$= \omega + f$

$c\Delta t^{S^*}$ = speed of light * satellite clock correction

where $\Delta t^{S^*} = \Delta t^S + \delta t^S$

$\varepsilon_{\substack{pseudo \\ range}}$ = measurement noise (uncertainty).

The "δ" in all cases represents the correction to the nominal.

3.3.2 Phase Range Measurement Model

The final model for the phase range (in meters) is given by Equation 3-20,

$$PR = \rho^* + c(t_R^* - t^S) + T^* - \frac{cI^*}{f^2} + (N\lambda)^* + S^* \sin\phi + C^* \cos\phi + c\Delta t^{S^*} + \varepsilon_{\substack{phase \\ range}} \quad (3\text{-}20)$$

where

$\rho^* = \sqrt{[x^S - (x_R - \delta x_R)]^2 + [y^S - (y_R - \delta y_R)]^2 + [z^S - (z_R - \delta z_R)]^2}$

= geometric distance between satellite at t^S and receiver at t_R

$c(t_R^* - t^S)$ = speed of light * clock differences due to clock inaccuracies

where $t_R^* = t_R - \delta t_R$

T^* = tropospheric correction from Hopfield model = $T - \delta T$

cI^*/f^2 = speed of light * ionospheric correction, scaled by the square of the frequency of the carrier (in MSOFE, nominal I = c(I - δI))

$(N\lambda)^*$ = integer ambiguity * wavelength of the carrier

S^* = arbitrary coefficient of the sine term = S - δS

C^* = arbitrary coefficient of the cosine term = C - δC

ϕ = location of the satellite in the orbital plane based on Keplerian elements

$= \omega + f$

$c\Delta t^{S^*}$ = speed of light * satellite clock correction

where $\Delta t^{S^*} = \Delta t^S + \delta t^S$

$\varepsilon_{\substack{phase \\ range}}$ = measurement noise (uncertainty)

The "δ" in all cases represents the correction to the nominal.

CHAPTER IV
RESEARCH AND RESULTS

4.1 Overview

This chapter is a summary of the research leading to this thesis. Descriptions of the measurement and bias models will be presented, as well as the state equations used to define the MSOFE "system" and "filter" models. The output of MSOFE will show the effects of different measurement and bias combinations on the "filter" performance due to higher-order error (random bias) sources present in the "system truth" model. Results will be presented as plots of the receiver's position uncertainty as a function of time.

This chapter will present the equations/models used by the computer program, MSOFE, for the implementation of the Kalman filter techniques. The problem-specific input required by MSOFE were[1]:

[1]Recall that MSOFE is a "shell" of an optimal Kalman filter processor. It consists of FORTRAN code divided up into a main program and 84 subroutines. Only 14 of these 84 were required to be changed to meet the special needs of the current user; these user-specific subroutines defined the state equations and measurement models for the system and filter. Other subroutines were written, as needed, to augment MSOFE and ensure all necessary information was available.

a. state dynamics (differential) equations,

b. measurement models,

c. partial derivative matrices (used in the linearization of the measurement models), and

d. the matrix to link the true value of the "filter" state vector to the "system truth" state vector model (called the "linear filter/system mapping matrix") (Carlson and Musick, 1990).

4.2 "System" versus "Filter"

The distinction between the "system" and the "filter" must be addressed for a complete picture of the processes behind MSOFE. As stated in Chapter 1, *within MSOFE*, the "filter" is the first-order representation of the real-world, and the "system" is the second-order representation. One may also think of the "filter" as an under-parameterized version of the over-parameterized "system." This thesis set out to examine the effects on the "filter" performance due to higher-order error/bias sources in the "system truth" model. One could think of the "system," in the context of MSOFE, as the truth or real-world model, perturbed by random effects with covariance **P**. The "filter" is the simpler model of the truth, containing a sufficient number of states to adequately represent the physical phenomena of interest. The *a priori* covariances within the "filter" will be much greater than those of the "system"; the purpose of the Kalman technique is to optimize the values for the desired quantities (i.e., states in the state vector) with the help of properly modeled measurements.

4.3 State Equation Models

The state equation formulation for input into MSOFE began with Equation 2-16, the (linearized) homogeneous differential equation of the error states with the presence of a noise input (recall from Section 2.3.2.1 that the system process noise matrix **G** = **I**), seen in Equation 4-1.

$$\delta\dot{\underline{x}} = \mathbf{F}\delta\underline{x} + \underline{w} \tag{4-1}$$

Matrix **F** in Equation 4-1 is the homogeneous state dynamics matrix, $\delta\underline{x}$ is the random system error state vector, and $\underline{w}$ is the white noise vector. The GPS system modeled in this thesis was modeled as a *random walk* (Gelb, 1992); therefore, Equation 4-1 becomes

$$\dot{\underline{x}} = \underline{w} \tag{4-2}$$

where **F** = [0], i.e., one assumes no knowledge about the dynamics of the problem. A random walk may be thought of as a system which makes fixed-length steps in arbitrary directions (ibid). Both the system truth and the filter models were modeled in this fashion. The noise vector $\underline{w}$, as $\mathbf{Q} = E[\underline{w}\underline{w}^T]$, was used by MSOFE in the covariance propagation equation for the operational Kalman filter, presented as Equation 2-28[2]. The **Q** matrix for the "system truth" was the zero matrix because

[2]Within MSOFE, the state and covariance dynamics equations are solved using a single-step numerical integrator that uses a Runge-Kutta type method.

the system was modeled as close to ideal (the truth) as possible and did not receive any deviations due to insufficient knowledge of the approximation process used in linearization. The "filter", on the other hand, *was* modeled with a process noise matrix. The presence of this matrix indicated that the filter output at time t+1 did not depend on the output at time t. In other words, the presence of the process noise indicated that the time sequences of the state vector and covariance contained insufficient information to predict their respective values from epoch to epoch. Only the states corresponding to the station position and clock contained process noise, implying that these four states were the unknown values to be determined by the filter. The "system truth" was modeled with extremely small *a priori* covariances (relative to the filter model), as these states are considered known.

The "system" and "filter" error state vectors initially will be identical (equal number of states in each). As biases are incorporated through the course of the research, the size of the system state error vector will grow, augmenting the "real-world" interpretation of the model. The mapping vector, mentioned above, will map the like states in the system error vector to the corresponding *true values* of the filter states in a one-to-one manner (Carlson and Musick, 1990), i.e., the mapping matrix will be defined by $\mathbf{A}_{fs}$ in Equation 4-3.

$$\underline{x}_f = \mathbf{A}_{fs}\underline{x}_s \tag{4-3}$$

Matrix $\mathbf{A}_{fs}$ will be of dimensions (number of filter states) x (number of system states). This matrix, in this research, will be defined as that matrix with elements A(n,n) = 1, and all other elements = 0.

4.4 Measurement Models

As stated before, two measurement types were used in this research: pseudorange and phase range. The most basic measurement type in GPS work is the pseudorange measurement. Therefore, all iterations of the program began with the baseline using pseudorange measurement data. To examine the effect of adding a more precise measurement type, the iterations were repeated using pseudorange and phase range together through the Kalman filter. Therefore, two measurement models were necessary. Table 2 shows the *measurement* models for the system/filter pseudorange and phase range[3]. The symbol "δ" indicates an entry in the "system" state vector (*true* error), and the "δ hat" indicates an entry in the "filter" state vector (*estimate* of the error). Measurement noise, v, (uncertainty) for the pseudorange measurements was set to $\pm$1 m, and measurement noise for the phase range measurements was set to $\pm$1 mm.

As mentioned previously in Chapter 3, because of MSOFE's unique approach to Kalman filtering, the "whole value" quantity supplied by the user is the "true" value; the state vector corrects this truth to become "nominal" (linearization takes

[3] Note that the measurement biases were added piecemeal, and the effect (output) was examined after each addition.

TABLE 2

GPS MEASUREMENT MODELS

Pseudorange Measurement, "System Truth" Model

$\underline{r}_R^S = \underline{r}^S - (\underline{r}_R - \delta\underline{r}_R)$	relative position from satellite (S) to receiver (R), R corrected for true error
$\rho = \lvert \underline{r}_R^S \rvert$	geometric range from S to R
$R_1 = \rho + c[(\Delta t_R - \delta t_R) - \Delta t^S]$	pseudorange measurement, time corrected for true error
$R_2 = R_1 + T[\text{scale} - \delta(\text{scale})]$	pseudorange plus tropospheric delay, corrected for *true error*
$R_3 = R_2 + I[\text{scale} - \delta(\text{scale})]$	pseudorange plus ionospheric delay, corrected for true error
$R_4 = R_3 + (A - \delta A)\sin\varphi + (B - \delta B)\cos\varphi + c\,(\Delta t^{SAT} - \delta t)$	pseudorange plus orbit biases, all corrected for true error
$R_5 = R_4 + (v_R * \Delta v_R)$	pseudorange plus measurement noise, scaled by a normal, Gaussian random number generator

Pseudorange Measurement, "Filter" Model

$\underline{r}_R^S = \underline{r}^S - (\underline{r}_R - \delta\underline{r}_R + \hat{\delta}\underline{r}_R)$	relative position from S to R, corrected for true error and best estimate of error
$\rho = \lvert \underline{r}_R^S \rvert$	geometric range from S to R

TABLE 2, continued

$R_1 = \rho + c[(\Delta t_R - \delta t_R + \hat{\delta} t_R) - \Delta t^S]$	pseudorange measurement, time corrected for true error and best estimate of error
$R_2 = R_1 + T[\text{scale}]$	pseudorange plus tropospheric delay
$R_3 = R_2 + I[\text{scale}]$	pseudorange plus ionospheric delay
$R_4 = R_3 + A\sin\varphi + B\cos\varphi + c\,\Delta t^{SAT}$	pseudorange plus orbit biases
$R_5 = R_4 + v_R$	pseudorange plus measurement noise

Phase Range Measurement, "System Truth" Model

$\underline{r}_R^S = \underline{r}^S - (\underline{r}_R - \delta\underline{r}_R)$	relative position from S to R, corrected for true error
$\rho = \lvert\, \underline{r}_R^S \,\rvert$	geometric range from S to R
$P_1 = \rho + c[(\Delta t_R - \delta t_R) - \Delta t^S]$	phase range measurement, time corrected for true error
$P_2 = P_1 + [N\lambda - \delta(N\lambda)]$	phase range plus integer ambiguity, corrected for true error
$P_3 = P_2 + T[\text{scale} - \delta(\text{scale})]$	phase range plus tropospheric delay, corrected for true error
$P_4 = P_3 + I[\text{scale} - \delta(\text{scale})]$	phase range plus ionospheric delay, corrected for true error
$P_5 = P_4 + (A - \delta A)\sin\varphi + (B - \delta B)\cos\varphi + c\,(\Delta t^{SAT} - \delta t)$	phase range plus orbit biases, all corrected for true error

TABLE 2, continued

$P_6 = P_5 + (v_p * \Delta v_p)$	phase range plus measurement noise, scaled by a normal, Gaussian random number generator

Phase Range Measurement, "Filter" Model

$\underline{r}_R^S = \underline{r}^S - (\underline{r}_R - \delta\underline{r}_R + \hat{\delta}\underline{r}_R)$	relative position from S to R, corrected for true error and best estimate of error
$\rho = \lvert \underline{r}_R^S \rvert$	geometric range from S to R
$P_1 = \rho + c[(\Delta t_R - \delta t_R + \hat{\delta} t_R) - \Delta t^S]$	phase range measurement, time corrected for true error and best estimate of error
$P_2 = P_1 + [N\lambda - \delta(N\lambda) + \hat{\delta}(N\lambda)]$	phase range plus integer ambiguity, corrected for true error and best estimate of error
$P_3 = P_2 + T[\text{scale}]$	phase range plus tropospheric delay
$P_4 = P_3 + I[\text{scale}]$	phase range plus ionospheric delay
$P_5 = P_4 + A \sin\varphi + B \cos\varphi + c\,\Delta t^{SAT}$	phase range plus orbit biases
$P_6 = P_5 + v_p$	phase range plus measurement noise

place around the nominal value). Recall Equation 3-18 which shows the relationship between the "truth", the "nominal", and the "correction". Using this logic, the "system" measurement model in MSOFE will correct the desired quantities as in Equation 4-4, and the "filter" measurement model as in Equation 4-5.

$$\text{SYSTEM: nominal} = \text{truth (whole value)} - \text{true error} \tag{4-4}$$

$$\text{FILTER: nominal} = \text{truth} - \text{true error} + \text{best estimate of the error} \tag{4-5}$$

Data used in the measurement models were simulated. All efforts were made to recreate as realistic a measurement value as possible. Twenty-eight possible satellite numbers were examined for each measurement type, for a total of 56 possible measurements. Obviously, all 28 satellite numbers did not contribute to the update, as information on every satellite was not included in the broadcast ephemeris. Not knowing in advance which satellites were listed in the ephemeris, provisions were made for all possible satellite combinations. Briefly summarized, here is a list of steps taken to generate the necessary information with which the range data were created within the software:

a. Broadcast ephemeris file was read [by the computer program] to calculate the nominal satellite position coordinates (per epoch), ionospheric correction coefficients, and the location of the satellites within the orbital plane (argument of latitude, ϕ).
b. Receiver data file for the corresponding broadcast ephemeris was read to return the nominal station coordinates.

c. Elevation of each satellite was calculated (per epoch).

d. Tropospheric delay of each satellite was calculated (per epoch), based on the elevation.

e. Ionospheric delay of each satellite was calculated (per epoch), based on the elevation.

f. Orbital errors for each satellite were calculated (per epoch), based on ϕ.

A point must be made concerning the epochs used in the research. Time tags of each epoch were incremented by MSOFE in order to update the state vectors and covariances. Updates were made every "second" (from 0 to 100 seconds), meaning that each "second," measurements were *taken*; at that time, an update was made. Time tags used to generate the measurements were updated each time a measurement was *needed*. In order to see a distinct movement of the satellites from the ephemeris file information, the time sent to the computer program's subroutines to calculate the measurements was incremented by 30 "seconds." In other words, the time used by MSOFE and that used by the measurement-generation routine were different, but they were each transparent to one another. The important aspect of the time definitions was to ensure that MSOFE and the measurement-generation routine conducted updates at the same instant--their relative times were, as such, unimportant.

In all cases, the station coordinates and the station clock correction were included in the filter and system state vectors. The *a priori* value for the standard deviations (in meters) of these quantities may be seen in Equation 4-6 and 4-7.

$$\left[\ \sigma_{\delta x} \quad \sigma_{\delta y} \quad \sigma_{\delta z} \quad \sigma_{\delta t}\ \right]^{T}_{system} = \left[\pm 1x10^{-4} \pm 1x10^{-4} \quad \pm 1x10^{-4} \pm 1x10^{-4}\right]^{T} \tag{4-6}$$

$$\left[\ \sigma_{\delta x} \quad \sigma_{\delta y} \quad \sigma_{\delta z} \quad \sigma_{\delta t}\ \right]^{T}_{filter} = \left[\pm 1x10^{-2} \pm 1x10^{-2} \quad \pm 1x10^{-2} \pm 1x10^{-2}\right]^{T} \tag{4-7}$$

For iterations containing phase range data, the integer ambiguity situation had to be addressed. The integer was considered an arbitrary number, so any value for an initial integer would have sufficed; an arbitrary value of $1x10^{6}$ was chosen for each satellite. The *a priori* standard deviation (in meters) of the integer ambiguity was chosen as $\pm 1x10^{-4}$ for the system and $\pm 1x10^{2}$ for the filter. This bias was present in both the "system" and "filter" state vectors, but only when phase measurements were processed.

The model for the tropospheric delay was taken from the Hopfield model (Goad and Goodman, 1974). The model creates the inverse relationship between the satellite's elevation and the correction due to the troposphere--the higher the satellite with respect to the station, the less the delay due to the troposphere. This inverse relationship is logical when one thinks of how the troposphere spans away from the earth's surface. If the satellite were high over the station, the GPS signal would travel less through the propagation medium to reach the receiver than if the

satellite were located on the horizon. The scale for the delay was chosen as 1.0. The entry in the state vector contained the uncertainty of the scale, as shown in Table 2. The *a priori* value for the standard deviation of the scale in the system model was chosen as ± 2 percent[4] (ibid). This bias was not included in the "filter" model.

The model for the ionosphere was taken from the ICD for the standard GPS receiver (Leick, 1990). This model, too, shows the inverse relationship between the elevation of the satellite with respect to the receiver and the amount of ionospheric delay. The scale for the delay was chosen as 1.0. The entry in the state vector contained the uncertainty of the scale, as shown in Table 2. The *a priori* value for the standard deviation of the scale in the system model was chosen as ± 50 percent (ibid). This bias was not included in the filter model.

The model for the orbit biases was taken from current theory of the perpetuation of errors in the orbit. This model constitutes a "once-per-revolution" effect of the perturbations of the Keplerian elements, which define the orbit of the satellite. The periodic oscillations of the satellite as it travels along its orbit and the deviation of the satellite clock are modeled in Equation 4-8. This model represents the change in the satellite-receiver range due to orbital biases. The argument of latitude (ϕ) places each satellite in its respective orbit. The clock term represents the deviation of the satellite clock from predicted models in the broadcast ephemeris

[4]Found by rms error of the Hopfield model divided by the average correction.

$$\Delta r = A \sin\phi + B \cos\phi + \Delta t^{satellite} \qquad (4\text{-}8)$$

information. Coefficients A and B represent the strength of each oscillation. In MSOFE, the coefficients were set to zero; the *a priori* value for the standard deviation of covariance of the coefficients was 10 m (initially, but other iterations were made with a deviation of ± 1 m, for comparison). The standard deviation of the satellite clock bias was initially set to ± 1 ns. These biases were only present in the "system" state vector.

As stated above, the computer program allowed for as many as 28 different satellite numbers. Therefore, 28 different measurements were possible when processing pseudorange data, and 28 were possible when processing phase range data. For the satellite-specific biases (integer ambiguity and the orbital biases), the state vector had to account for one state per possible satellite. Table 3 shows the size of the "filter" and "system" state vectors as the number of measurement biases changed. The integer ambiguity bias was not present in the state vectors for iterations using pseudorange data only.

The last condition investigated was that of cycle slips. As mentioned before, a cycle slip occurs when the signal from satellite to receiver is--for whatever reason--disrupted. This disruption often stems from an actual, physical blocking of the signal from, for example, a tree or building, or perhaps the GPS receiver on an aircraft is blocked from the signal's path by the plane's own maneuvering. In the filter, the cycle slip was simulated by setting up a flag to look for Satellite #3 during

epochs 3, 20, and 70. When these times occurred, a large value for **Q**, the process measurement noise, was inserted in the program associated with Satellite #3. The large noise value told the program that this value was now unknown (at those state epochs), and the effect of the slip was analyzed on output of the filter.

TABLE 3

STATE VECTOR ENTRIES PER INPUT

BIAS	SYSTEM VECTOR	FILTER VECTOR
x coordinate	1	1
y coordinate	1	1
z coordinate	1	1
receiver clock	1	1
integer ambiguity	28	28
troposphere	1	not present
ionosphere	1	not present
orbit (sine term)	28	not present
orbit (cosine term)	28	not present
satellite clock	28	not present

4.5 Results

This section will present the results of the iterations through the Kalman filter program as measurement type and biases were varied. The presentation of the output will be categorized by bias type. Then, comparisons will be made between the pseudorange and pseudo/phase range combinations. The different system state vector input combinations for each output graph may be seen in Tables 4, and 5[5]. The reader is referred to the end of this chapter for all output figures.

4.5.1 Geometry and Dynamics

An important aspect of GPS theory is the relationship of the satellites to the respective receiver. The geometry of one with respect to the other plays a major role in the user's ability to recover the receiver's position. Recall that the broadcast ephemeris was incremented in time to simulate the movement of the satellites. Two-dimensional plots of the satellites' location relative to the receiver may be seen in Figures 8, 9, 10, and 11[6]. The figures show the satellites' relative locations at four instances in the time interval of study. Without the presence of any other anomalies, the relative spacing of the satellites at times 1 and 60 seconds (Figures 8 and 9, respectively) would indicate a better possibility for recovering one's position with greater certainty. Further, the presence of a fifth satellite at t=60 sec further

[5]Not all combinations of biases and measurement types are presented here. Often, changing a variable did not appreciably change the output--these plots were not included because they did not offer any significant findings.

[6]Station and satellite coordinates were presented in the *topocentric* system.

TABLE 4

SYSTEM INPUT DEFINITION FOR EACH FILTER OUTPUT

Figure Numbers 14 through 29

SYSTEM SET-UP	FIGURE # (OUTPUT)	14	15	16	17	18	19	20	21	22	23	24	25	26	27	28	29
MEASUREMENT TYPE & DYNAMICS	pseudo range only	x	x	x	x	x				x	x		x		x	x	x
	pseudo & phase range	x	x				x	x	x	x		x		x			
	stationary case	x															
	moving case		x	x	x	x	x	x	x	x	x	x	x	x	x	x	x
STATION-DEPENDENT BIASES	station coords and clock	x	x	x	x	x	x	x	x	x	x	x	x	x	x	x	x
OBSERVATION-DEPENDENT BIASES	integer ambiguity						x	x	x	x		x		x			
	error-free troposphere			x	x	x	x	x	x	x	x	x	x	x	x	x	
	error on toposphere			x	x	x	x	x	x	x	x	x	x	x	x	x	x
	error-free ionosphere			x	x	x	x	x	x	x	x	x	x	x	x	x	
	error on ionosphere			x		x	x		x	x	x	x	x	x	x	x	
SATELLITE-DEPENDENT BIASES	error-free orbit	x	x	x	x	x	x	x	x	x	x	x	x	x	x	x	x
	error on orbit														x	x	x
	orbit coefficient = 10 m														x		x
	orbit coefficient = 1 m															x	x
	error on one satellite only																
MISCELLANEOUS	elev-dependent (tropo)										x	x					
	elev-dependent (ionos)												x	x			x

TABLE 5

SYSTEM INPUT DEFINITION FOR EACH FILTER OUTPUT

Figure Numbers 30 through 39

SYSTEM SET-UP	FIGURE # (OUTPUT)	30	31	32	33	34	35	36	37	37	39
MEASUREMENT TYPE & DYNAMICS	pseudo range only										
	pseudo & phase range	x	x	x	x	x	x	x	x	x	x
	stationary case (sta & sat)										
	moving case (sta & sat)	x	x	x	x	x	x	x	x	x	x
STATION-DEPENDENT BIASES	station coords and clock	x	x	x	x	x	x	x	x	x	x
OBSERVATION-DEPENDENT BIASES	integer ambiguity	x	x	x	x	x	x	x	x	x	x
	error-free troposphere	x	x		x	x	x	x	x		x
	error on toposphere	x	x	x	x	x	x	x	x	x	x
	error-free ionosphere	x	x		x	x	x	x	x		x
	error on ionosphere	x	x	x	x	x	x	x	x	x	x
SATELLITE-DEPENDENT BIASES	error-free orbit	x	x	x	x	x	x	x	x	x	x
	error on orbit	x	x	x	x			x	x	x	
	orbit coefficient = 10 m	x		x	x			x		x	
	orbit coefficient = 1 m		x	x					x	x	
	error on one satellite only				x						
MISCELLANEOUS	elev-dependent (tropo)										
	elev-dependent (ionos)			x			x			x	x
	equal msmt uncertainties					x	x	x	x	x	x
	cycle slip										x

increases the station/satellite polyhedron's "volume" (mentioned in Chapter 3), possibly leading to an even better position recovery. Figures 10 and 11 show the geometry begin to degrade as the satellites move topocentrically away from the receiver. One would expect, in an ideal situation, the position uncertainty to increase as the geometry degrades.

In addition to the geometry of the satellites and the receiver, the elevation of the satellite with respect to the receiver is also an important issue. The reader is referred to Figures 12 and 13, plots of the satellites' elevation and elevation versus azimuth, respectively, over the study interval. This plot was generated using the information from the broadcast ephemeris[7]. As stated above, the amount the GPS signal is affected by the propagation media is inversely proportional to the sine of the satellite's elevation. One may expect the position uncertainty to increase as the elevation angles decrease due to the larger bias affecting the measurement.

The data reduction through MSOFE began with the non-practical case of a non-moving receiver with non-moving satellites. In this case, station and satellite approximate coordinates were hard-programmed into MSOFE (were not taken from the ephemeris, as on subsequent runs). The purpose was to examine the uncertainty of the station's position when pseudorange measurements only were processed, with no external influences. Next, the consequence of adding phase range measurements was examined. Figure 14 shows the results. The plot of pseudorange only shows a

[7]The satellite numbers shown are those with data present in the ephemeris whose elevation was greater than a pre-defined cut-off value of 0 degrees.

steady uncertainty, logical because the station and satellite were stationary. The addition of the phase ranges immediately improves the overall uncertainty of the position; the phase bias for each satellite contributes a standard deviation at the rate of $1/\sqrt{n}$ where n is the number of measurements made.

In Figure 15, the station and satellite coordinates were taken from the broadcast ephemeris, varied with time. Due to the degradation of the geometry, the uncertainty of position using the pseudoranges-only model increases from t=0 to about t=83. The slight "glitch" at t=58 is due to the addition of the fifth satellite. The uncertainty of position decreases for (1-2 seconds) a small amount due to the added redundancy[8], but the low elevation of this fifth satellite and the further degradation of the geometry is counter-productive in keeping the uncertainty to within acceptable levels. The incorporation of the phase range clearly enhances the system, and the position uncertainty at the end of the study time approaches the millimeter level. The continued rising of satellites #12 and 16 (see Figure 12) past t=83 helps to further reduce the uncertainties.

4.5.2 Propagation Media

The next stage of study was to add the effects of the propagation media. Four iterations were made for each type of measurement--with and without tropospheric

[8]Recall that the quantities being estimated are the station coordinates and the station clock correction. A minimum of four satellites are required to solve for the four unknowns. Any satellites beyond the required four create a redundant situation and should decrease uncertainties, providing all other variables (elevation, propagation media delay, etc.) are also acceptable.

biases, and with and without ionospheric biases. Table 6 shows the four combinations and their other names that will be used interchangeably throughout this thesis.

TABLE 6

PROPAGATION MEDIA COMBINATIONS

COMBINATIONS	ALTERNATE NAME
ERROR-FREE TROPOSPHERE ERROR-FREE IONOSPHERE	IDEAL CASE (IDEAL/ DUAL-FREQUENCY)
ERROR ON TROPOSPHERE ERROR-FREE IONOSPHERE	DUAL-FREQUENCY CASE
ERROR-FREE TROPOSPHERE ERROR ON IONOSPHERE	< NONE >
ERROR ON TROPOSPHERE ERROR ON IONOSPHERE	REAL-WORLD CASE (SINGLE-FREQUENCY CASE)

The "ideal" case contains no propagation media errors. The dual-frequency case is so named because with a dual-frequency GPS receiver, it is possible to eliminate the linear affects of the ionosphere using post-processing measurement models (due to the *dispersive* characteristics of the ionosphere). The third combination is not practical in the real world--the effect due to troposphere cannot be eliminated while

the ionospheric effect remains. This combination was produced for comparison purposes only and will not be discussed in detail[9]. The "real-world" case is so named because it contains errors on both media. It is also known as the single-frequency case because both biases will be present with a single-frequency receiver (neither can be eliminated without further information).

Figure 16 shows the effect of the propagation media on the model containing only pseudorange measurements. The ideal case (no errors on either) is the same plot as seen in Figure 15. The effect of adding the troposphere, known to 2%, to get the dual-frequency model only increases the uncertainty by less than 0.1 m, shown in Figure 17[10]. However, adding the ionospheric bias with a standard deviation of 50% increases the uncertainty by approximately 2.5 m. In the single-frequency plot, the "glitch" at t=58 sec is more pronounced than that in the plot void of these biases, more clearly seen in Figure 18. Recall at t=58 that the elevation of the fifth satellite rises to above 0 degrees and enters into the filtering process. The low elevation contributes a large amount of delay to the measurement (about 84 m tropospheric correction and 21 m ionospheric correction). The redundancy of the additional satellite is not enough to counteract the large contribution of the propagation media, so the uncertainty rises by approximately 2 m. Contrast this jump in uncertainty to the slight decrease of uncertainty in the ideal case, where

---

[9]This combination typically showed little difference from the ideal case due to the small ($\pm$2%) uncertainty on the tropospheric delay.

[10]NOTE: The graphs with and without the tropospheric bias (with the same ionospheric biases) were essentially the same. The plots were offset slightly on the plot so that the four plots could be distinguished from one another.

elevation does not play a role in determining the uncertainty. Subsequent to t=58, the degrading geometry somewhat blends with the effect of elevation, i.e., satellites #3, 17, and 26 are sufficiently high above the receiver so to not degrade the uncertainty, despite the geometry.

The addition of phase ranges to the pseudorange measurements may be seen in Figure 19 for all four combinations of propagation biases. The ideal case is the same plot as seen in Figure 15. Despite the mm-level measurement noise of the phase range measurements, the addition of the tropospheric bias creates a pronounced increase in the position uncertainty. From t=0 to t=58 sec, the ideal case and the dual-frequency case are identical at the millimeter level (see Figure 20 for a clearer look at the two graphs). With the addition of the fifth satellite, the redundancy cannot make up for the low elevation and the associated large uncertainties imposed on the measurements. Figure 21 shows the ideal case versus the real-world case. The addition of tropospheric and ionospheric biases to the combined pseudo/phase range model greatly increases the uncertainty of the receiver's position. The redundancy of one satellite cannot correct for the large contribution the satellites' elevations pay toward the uncertainty. The three setting satellites and the low (redundant) satellite contribute too much uncertainty to the problem.

Figure 22 provides a look at the comparison between the two measurement types. Between t=0 and t=58 sec, the pseudo/phase range combination provides better results than the pseudorange-only model. After t=58 sec, the pseudorange-

only case is comparatively unaffected by the poor geometry and low elevation angle of the redundant satellite. However, the pseudo/phase range model shows a greater reaction to the elevation-dependent biases. Recall from Chapter 3 that the ionosphere affects the phase and pseudorange values in opposite directions. The combination of the two measurement types actually magnifies the effect of the bias on the recovered position uncertainty. As the fifth satellite rises to a more acceptable level (around 10 degrees elevation), and the maintenance of three other satellites at acceptable elevations, the pseudo/phase range and the pseudorange-only cases approach the same level of uncertainty.

4.5.3 Elevation-Dependency

Due to the results of the propagation media models in the previous section, another model was developed--the elevation-dependent model. Two models were developed: one based on the tropospheric correction values and one based on the ionospheric correction values. In these models, the measurement noise was weighted to give less emphasis to those satellites with low elevation angles and more emphasis to those with higher elevation angles. The new uncertainty may be seen in Equations 4-9 and 4-10 for the tropospheric-dependent and ionospheric-dependent models, respectively,

$$\sigma_{revised} = \sqrt{(\sigma_{msmt})^2 + (\sigma_{tropo})^2} = \sqrt{(\sigma_{msmt})^2 + (0.02T)^2} \qquad (4\text{-}9)$$

$$\sigma_{revised} = \sqrt{(\sigma_{msmt})^2 + (\sigma_{ionos})^2} = \sqrt{(\sigma_{msmt})^2 + (0.5I)^2} \qquad (4\text{-}10)$$

where T and I are the calculated values for the tropospheric and ionospheric corrections, respectively, and the σ_{msmt} is the standard deviation of the measurement (phase range or pseudorange). Using these models, one can see that the combined deviation will be greater than that of just the measurement deviation. The standard deviation of the measurement noise will be used to calculate the filter updates per the Kalman update equations and will have an overall effect of $\mathbf{R}^{-1}$ (inverse of the measurement noise matrix, see Chapter 2) on the update. Therefore, satellites with large tropospheric/ionospheric corrections will contribute less to the process.

Because the problem requires four satellites to determine uniquely the four unknowns, no change in the output of the filter should be expected when only four satellites are present. Therefore, the weightings will only come into play with the addition of the redundant satellite(s). One would expect, therefore, to see little change in the uncertainty curves (with and without the model) up to t=58 sec, and the addition of Satellite #12 beyond t=58 should improve the uncertainty results.

4.5.3.1 Dependency Based on Troposphere

Figure 23 shows the pseudorange-only uncertainty curves with the measurement noise dependent on the tropospheric corrections. As expected, the uncertainty curves for the real-world cases with and without the elevation dependency do not differ when only four satellites are visible above the horizon. However, with the addition of the fifth satellite, the position uncertainty does

decrease, albeit only slightly. The small uncertainty of the troposphere correction (only $\pm 2\%$) does not play an extensive role in the weighting of the measurement noise, and not much improvement is noted.

Figure 24 shows the pseudo/phase range uncertainty curves with the measurement noise dependent on the tropospheric corrections. As expected, there is no change in the uncertainty curves with and without the elevation-dependent model through t=58 sec. Dramatic results occur, however, after t=58. The large spike in the uncertainty after the addition of the fifth satellite does not occur in the elevation-dependent model. Instead, the uncertainty curve is smooth; the weighting of the lowest (in elevation) satellite's measurement plays down the importance of this measurement. The dip in the elevation-dependent curves at approximately t=86 sec occurs near the point where Satellites #12 and #16 reach equal elevations. The weighting tends to create a non-optimal geometry by de-emphasizing the measurements from the satellites with the lowest elevation. Past t=86 sec, the measurement from Satellite #12 is de-emphasized. If one recalls Figure 10, the geometry of the station and satellites, one can see the effect on the geometry of (essentially) removing Satellite #12. The "polyhedron" is greatly reduced in size, thereby increasing the position uncertainty. Past $t \approx 95$ sec, the measurement for Satellite #16 is de-emphasized; one can see from Figure 11 the effect on the geometry of eliminating Satellite #16 at this time. Here, the implementation of the elevation-dependent measurement noise model does not produce optimum uncertainty results. The three setting satellites and the degrading geometry cannot

be compensated for in the elevation-dependent model, and the elevation-independent model yields more realistic results.

4.5.3.2 Dependency Based on Ionosphere

Figure 25 shows the elevation-dependent measurement noise model, based on the ionospheric correction, in the pseudorange-only measurement. Just as for the troposphere-dependent model in Figure 23, the elevation-dependent and independent models are identical prior to t=58 sec. Subsequent to t=58, in the presence of the redundant satellite, the uncertainty increases. Clearly, there is a trade-off between weighting of the measurements and the uncertainty of the position. By giving less weight to the lowest (elevation) satellite, the geometry is degraded, and the uncertainty increases.

In Figure 26, the elevation-dependency is based on the ionospheric correction model, and the measurement model is the pseudo/phase range combination. Here, the presence of the phase range measurements slightly increases the uncertainty (less than 1 m) for epochs prior to t=58 sec. However, after t=58 sec, the elevation-dependent model yields improved results. There is still some trade-off in the geometry at epochs greater than 97 sec, but overall, the uncertainty is improved with the elevation-dependent model. The addition of phase ranges adds to the improvement over the case seen in Figure 25.

4.5.4 Orbital Biases

The orbital errors were added in two different ways. First, the trigonometric coefficients were given an *a priori* standard deviation of ± 10 m. Second, the trigonometric coefficients were given a standard deviation of ± 1 m. In both cases, the satellite clock was given an *a priori* standard deviation of ± 1 ns. Each way will be addressed.

Figure 27 shows the pseudorange-only case for the $\sigma = \pm 10$ m case. The measurement models with and without the orbital errors are contrasted. The figure clearly shows that the large uncertainty of the orbit contributes to the increased uncertainty of the position of the station. The increase in uncertainty is approximately ten-fold at its peak, at approximately t=83 sec. In Figure 28, the standard deviation of the orbital bias coefficient is set to ± 1 m. Obviously, knowing the coefficients ten times better serves to reduce the uncertainty in the position by approximately the same amount at its peak (around t=83 sec).

Figure 29 shows the real-world model using pseudoranges only and an elevation-dependent measurement noise model, based on the ionosphere. Curves with both values for and without the orbital bias are shown. The addition of the elevation-dependency model in concert with the orbital bias problem did not change the plots from those seen in Figures 27 and 28. The presence of the orbit error was significant enough to override the weighting of the lower satellite. No significant value was gained by using the elevation-dependency model in this case.

In Figure 30, the addition of phase ranges to the "filter" observation model vastly improves the uncertainty over the pseudorange-only case of Figure 27. In Figure 30, the orbit bias using a coefficient $\sigma = \pm 10$ m, through t=58 sec, is identical to the uncertainty curve of Figure 27 (pseudorange only). With the addition of the redundant satellite, the uncertainty drops markedly and follows the same shape as the model without the orbital errors. In contrast to the curve void of orbital biases, the uncertainty curve with the orbital bias differs by only as much as 9 m at its largest point, a stark improvement from the comparison shown in Figure 27. Although the orbital bias adds uncertainty to the position of the station, the addition of phase ranges improves the results overall.

In Figure 31, the curves found using $\sigma = \pm 1$ m are all virtually identical prior to t=58 sec. The addition of the orbit errors subsequent to that time yields results which parallel those of the no-orbit-bias curve. The presence of the redundant satellite does not counteract the presence of the tropospheric, ionospheric, and orbital biases.

Figure 32 looks at the situations already shown in Figures 30 and 31, except with the presence of the elevation-dependent measurement noise model based on the ionosphere. The combination of the uncertainty in the ionosphere together with the ionospheric, tropospheric, and orbital biases creates a situation which produces an unacceptable uncertainty curve when compared to other schemes.

Figure 33 investigates the contribution of one satellite, here Satellite #3, infected with orbital biases, where the orbit coefficients' *a priori* $\sigma = \pm 10$ m for Satellite #3, and $\sigma = \pm 1 \times 10^{-20}$ m for all other satellites. The overall uncertainty curve found from a biased Satellite #3 is seen to contribute approximately 10 m to the case without orbital biases.

4.5.5 Equal Measurement Noise

The next situation examined was that of equal measurement noise. Both the pseudorange and phase range measurements were assigned a measurement noise of ± 1 m in the filter model. Figure 34 may be compared to Figure 21. In Figure 34, the presence of the equal measurement noise does not improve the uncertainty from the beginning for the ideal case. For the single-frequency model, the curve in Figure 21 and Figure 32 are identical up until t=58 sec. Although the "spike" from Figure 21 does not appear after that time, the equal-noise case does not lead to the improved uncertainty in the face of the degraded geometry as time approaches t=100 sec.

In Figure 35, the elevation-dependent (based on the ionosphere) model is examined. There is definitely a trade-off past t=58 sec in the uncertainty curves for the elevation-dependent and -independent models. As the geometry degrades, the uncertainty improves with the former model; the latter model sees the better results as the redundant satellite rises in the sky, but before the geometry degrades. As in

Figure 34, the equal measurement noises do not serve to improve the overall output of the filter, hence the uncertainty of the station's position.

In Figures 36 and 37, the orbital errors are introduced ($\sigma = \pm 10$ and ± 1 m, respectively). The uncertainty curve resembles those in Figures 27 and 28, respectively, for the pseudorange-only case. The uncertainty in Figure 36 at its peak is slightly better than in Figure 27, possibly due to the increased number of measurements in the pseudo/phase range situation and the differences in the measurement models for each case. The same case could be made for Figures 37 and 28.

Figure 38 shows the case in Figure 36 with the elevation-dependent (based on ionosphere) model. This curve resembles that of Figure 32, but this curve peaks at a smaller uncertainty value, for the reasons mentioned above.

4.5.6 Cycle Slip

One final iteration was made for this problem. The issue of cycle slips, or losses of lock, was analyzed. Figure 39 shows the results of placing a simulated cycle slip at t = 3, 20, and 70 seconds. When only four satellites are visible, the cycle slip has no affect on the uncertainty curve. By introducing a cycle slip, the program is being told of another unknown state. This fifth unknown cannot be resolved until such time as a fifth satellite comes into view, making the system solvable. The cycle slip, because it is introducing an uncertainty in the integer

ambiguity value, causes an increase in the overall uncertainty of the position. The effect of the slip at t=70 seconds can clearly be seen in the single-frequency case. The uncertainty curve for the ideal case, that without tropospheric and ionospheric delay biases, is not effected by the slip.

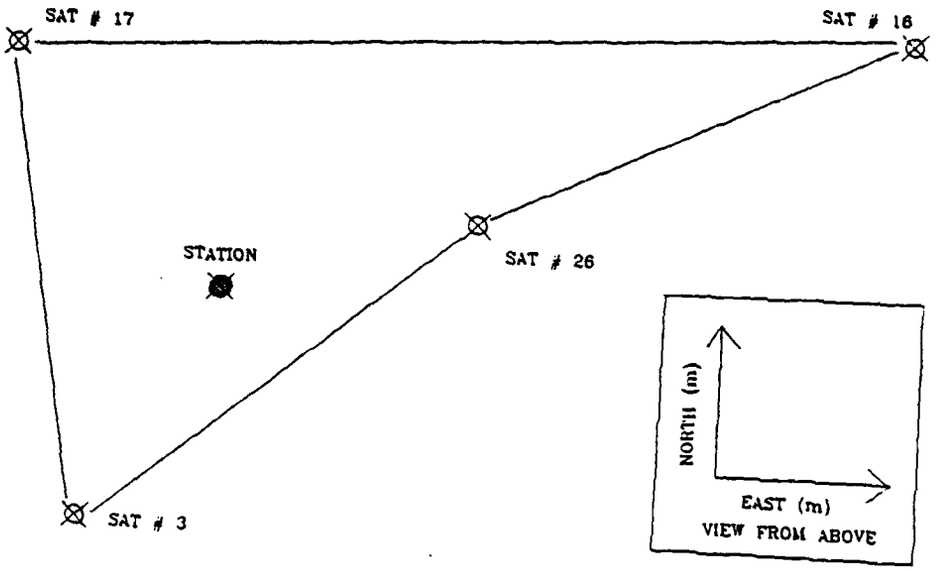

FIGURE 8

GEOMETRY OF THE SATELLITES

RELATIVE TO THE STATION

Time = 1 second

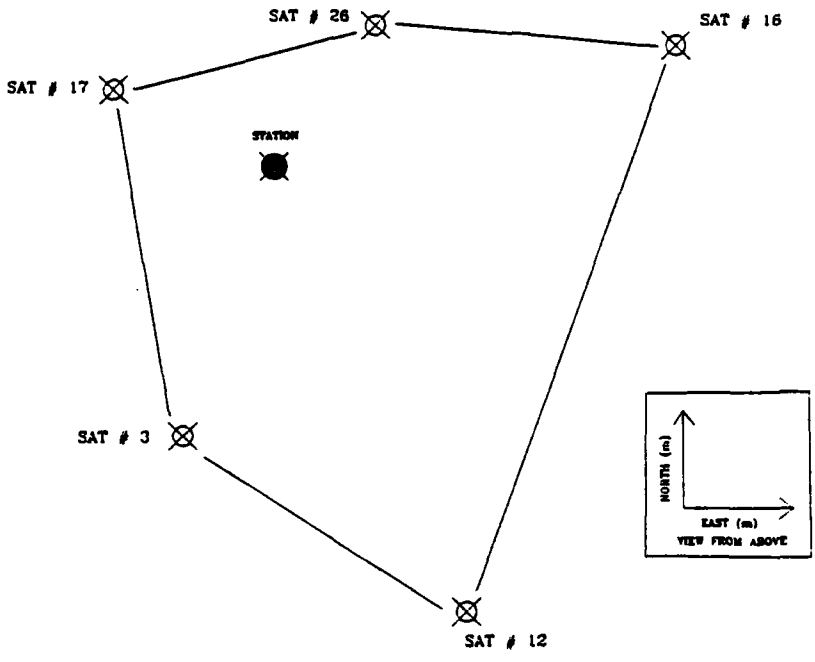

FIGURE 9

GEOMETRY OF THE SATELLITES

RELATIVE TO THE STATION

Time = 60 seconds

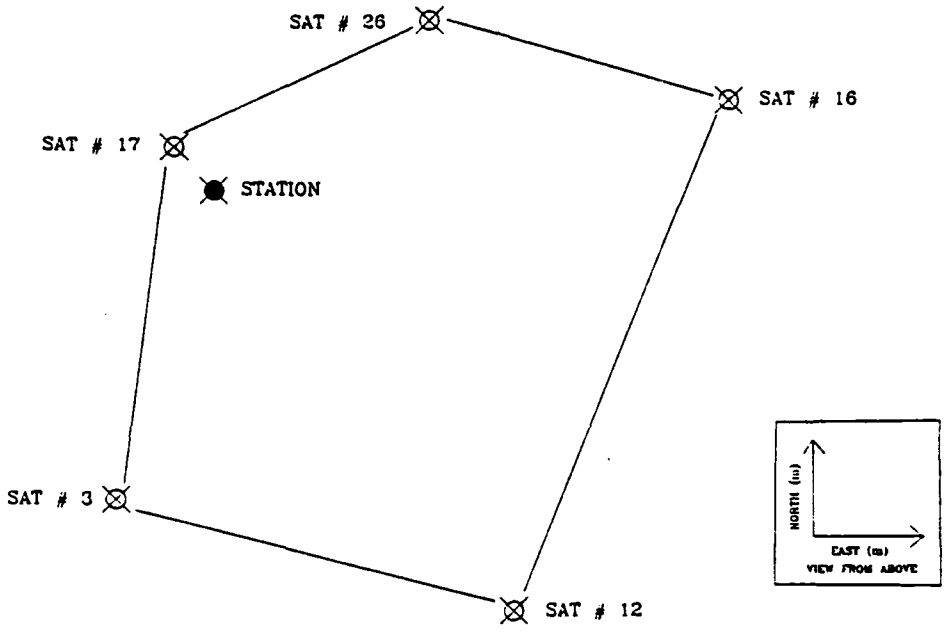

FIGURE 10

GEOMETRY OF THE SATELLITES

RELATIVE TO THE STATION

Time = 83 seconds

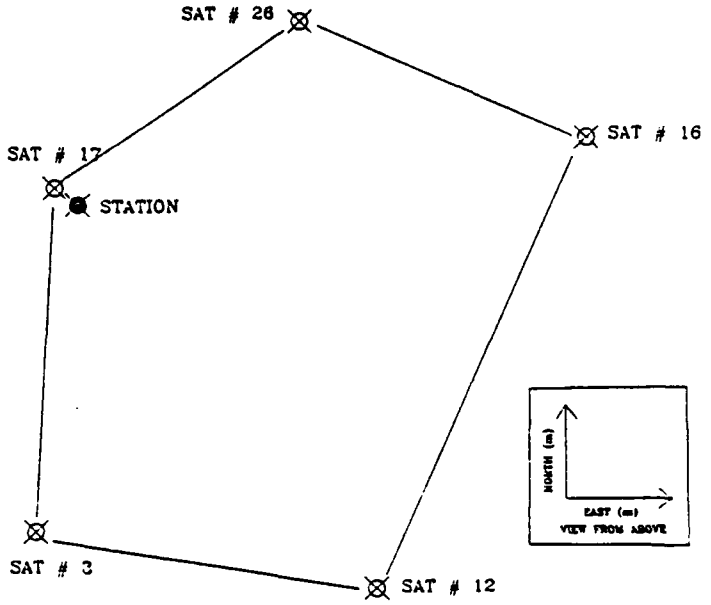

FIGURE 11

GEOMETRY OF THE SATELLITES

RELATIVE TO THE STATION

Time = 100 seconds

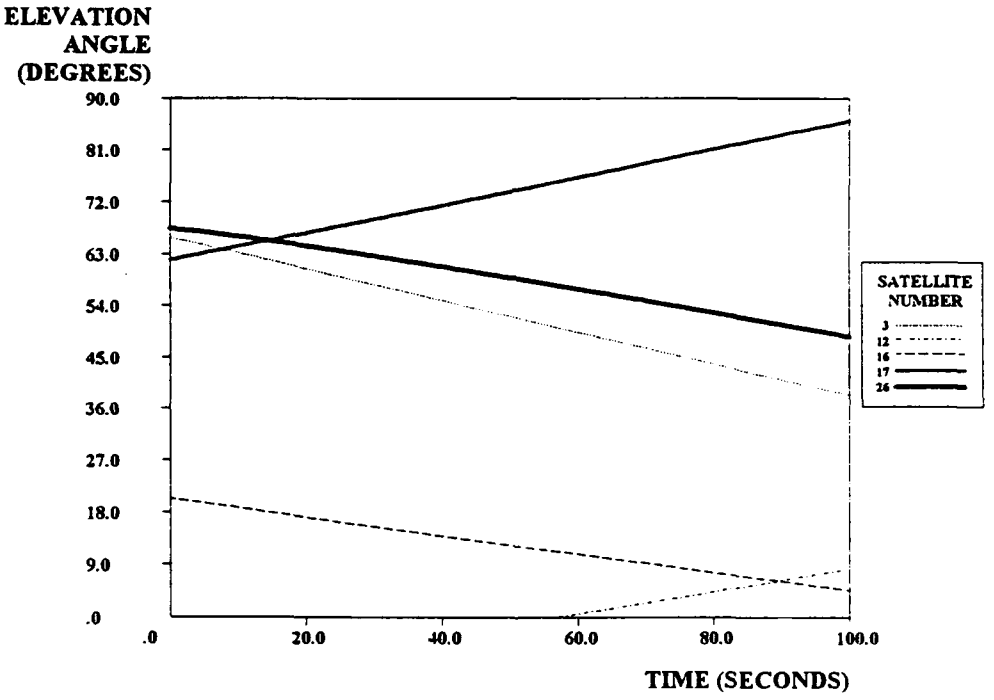

FIGURE 12

SATELLITE ELEVATION ANGLE OVER TIME

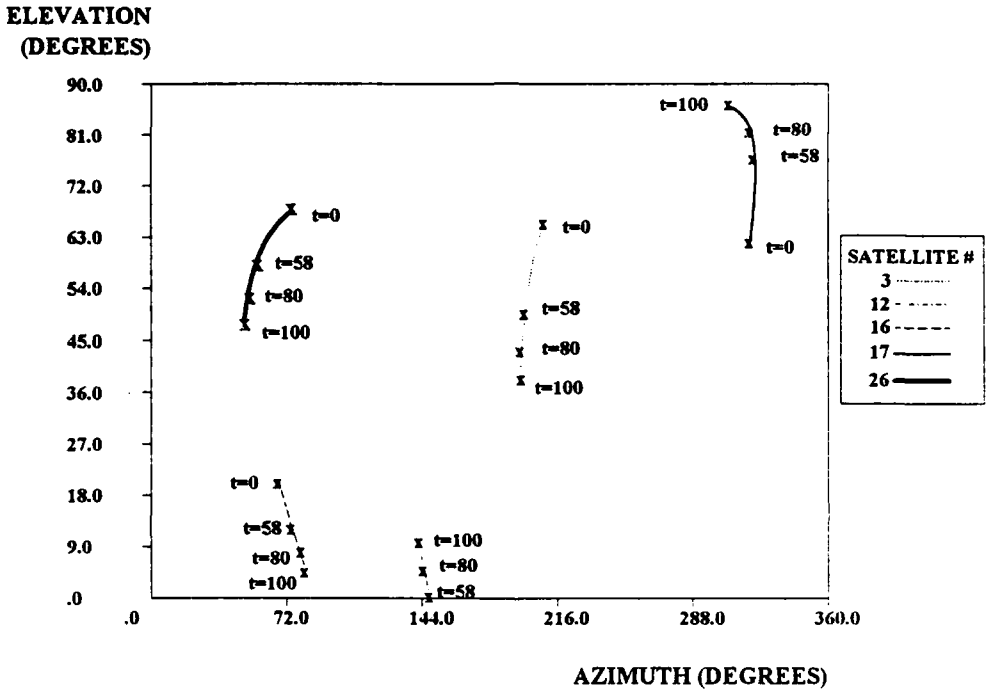

FIGURE 13

SATELLITE AZIMUTH VERSUS ELEVATION OVER TIME

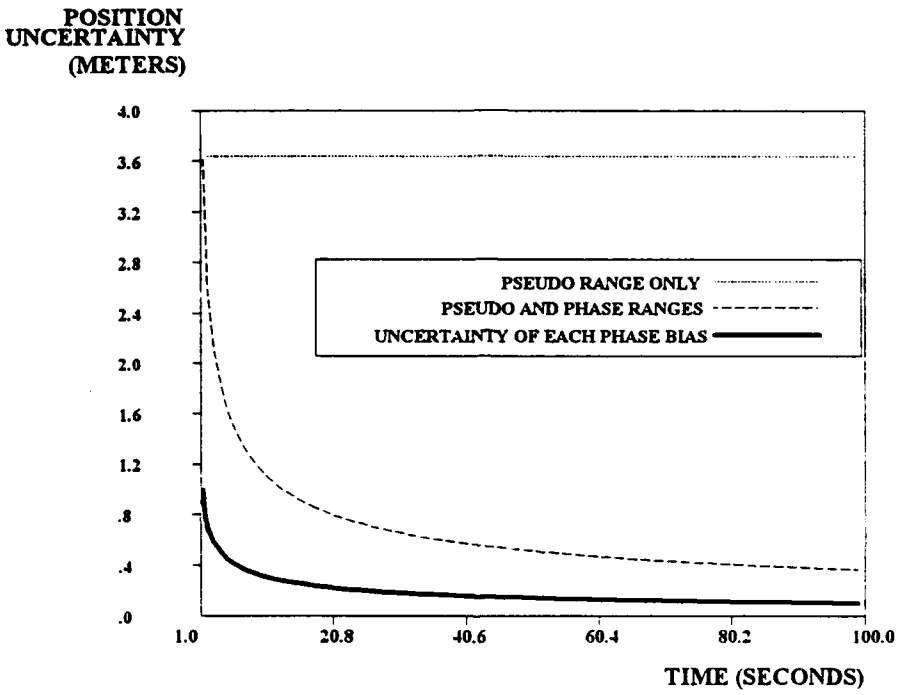

FIGURE 14

UNCERTAINTY USING PSEUDO AND PHASE RANGES

Stationary Satellite and Station

Ideal Case

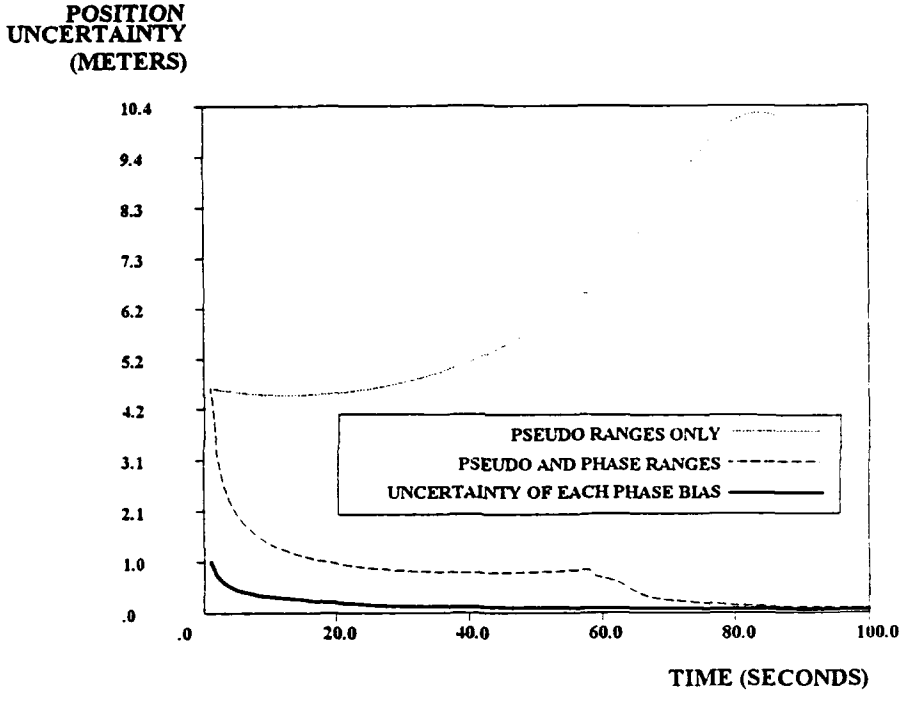

FIGURE 15

UNCERTAINTY USING PSEUDO AND PHASE RANGES

Moving Satellite and Station

Ideal Case

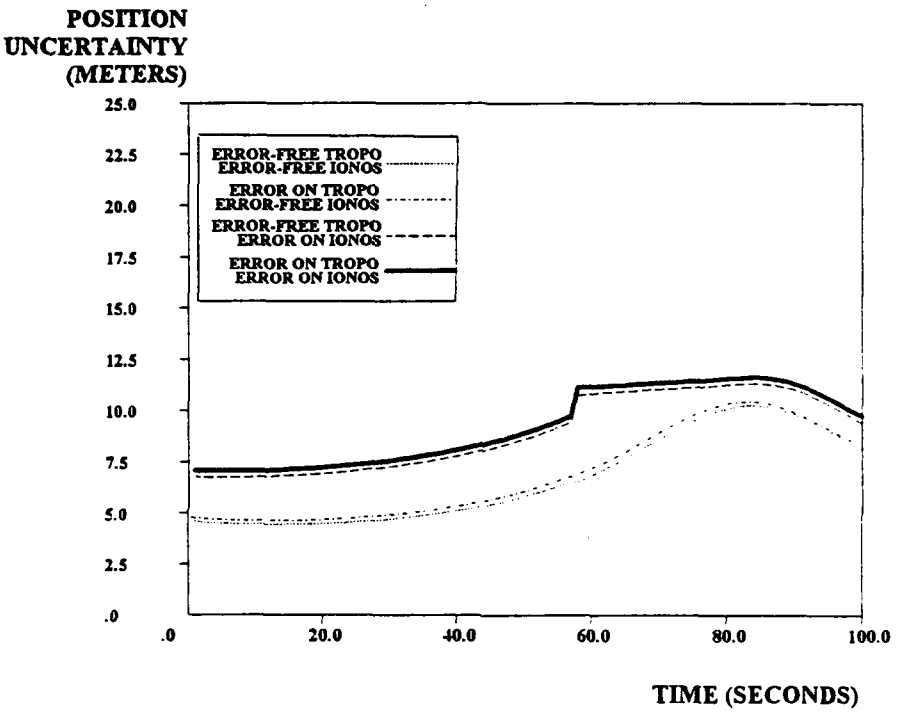

FIGURE 16

UNCERTAINTY USING PSEUDO RANGES

w/ and w/o Tropospheric and Ionospheric Errors

Single- and Dual-Frequency Models

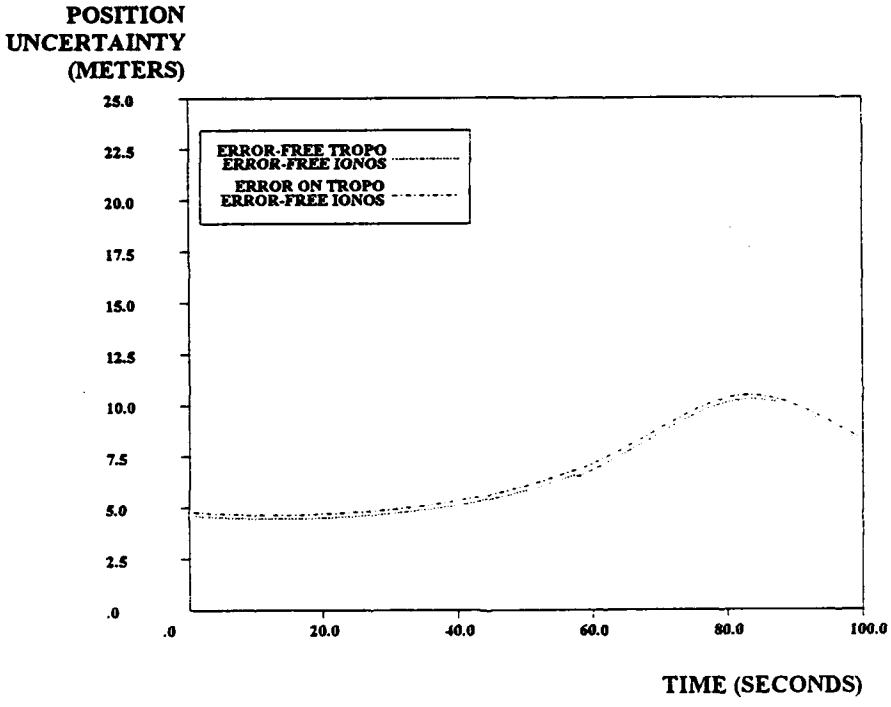

FIGURE 17

UNCERTAINTY USING PSEUDO RANGES

w/ and w/o Tropospheric Errors

Dual-Frequency Model

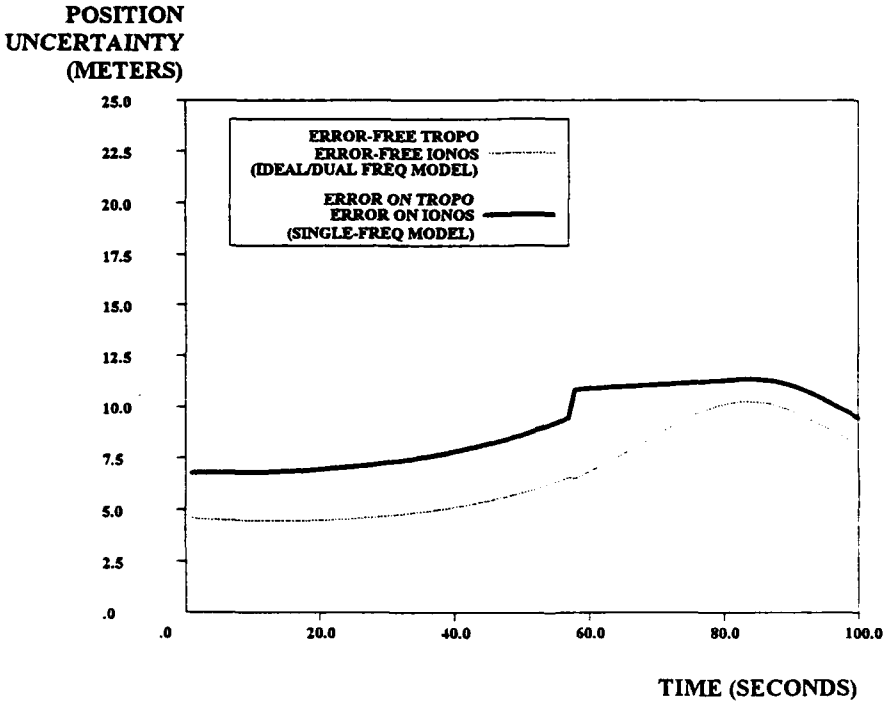

FIGURE 18

UNCERTAINTY USING PSEUDO RANGES

Ideal Case vs. Real World Case

Single- and Dual-Frequency Models

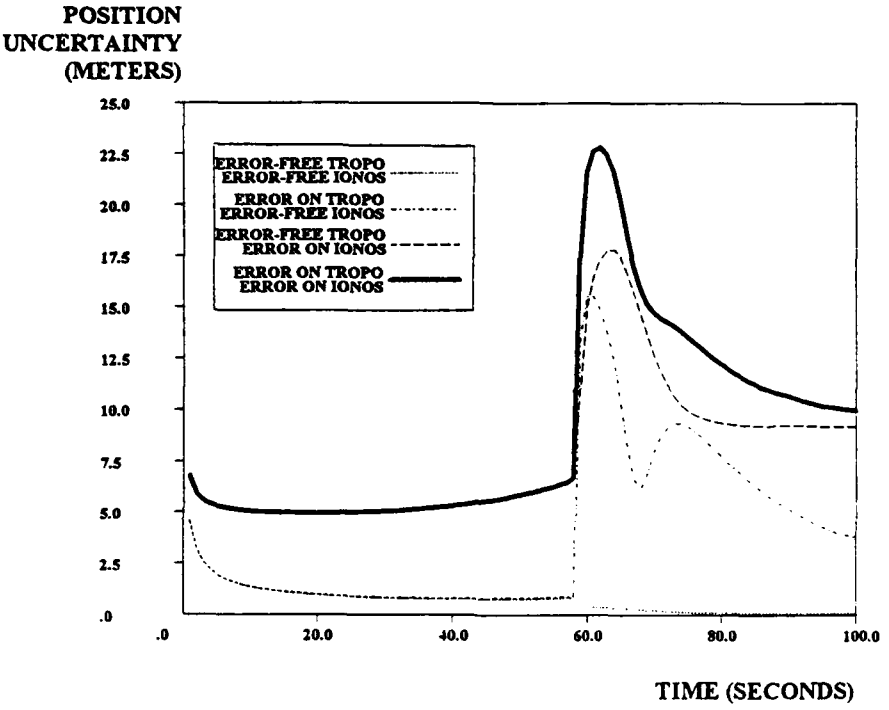

FIGURE 19

UNCERTAINTY USING PSEUDO AND PHASE RANGES

w/ and w/o Tropospheric and Ionospheric Errors

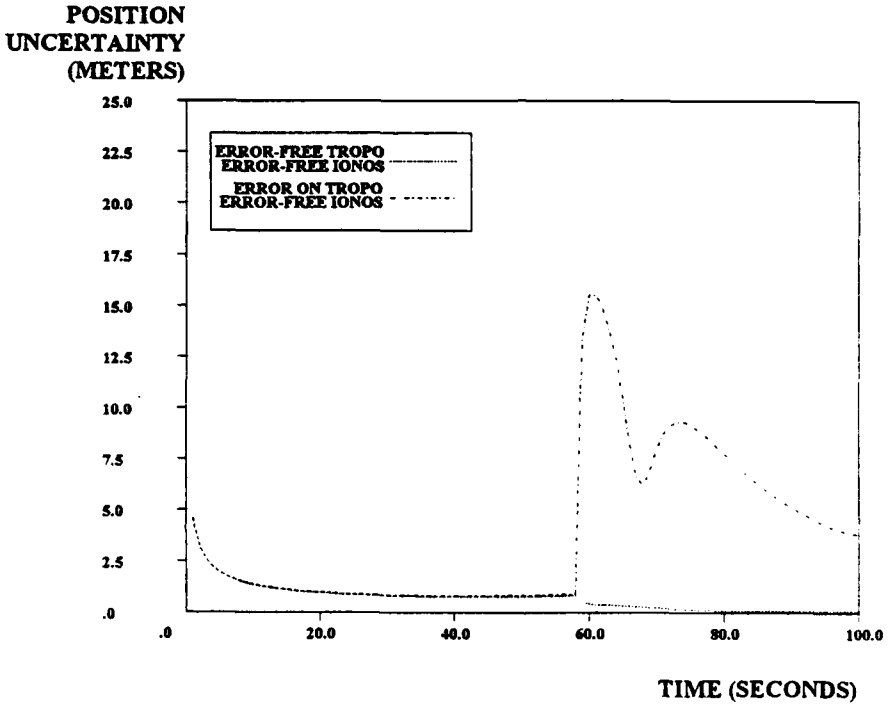

FIGURE 20

UNCERTAINTY USING PSEUDO AND PHASE RANGES

w/ and w/o Tropospheric Errors

Dual-Frequency Model

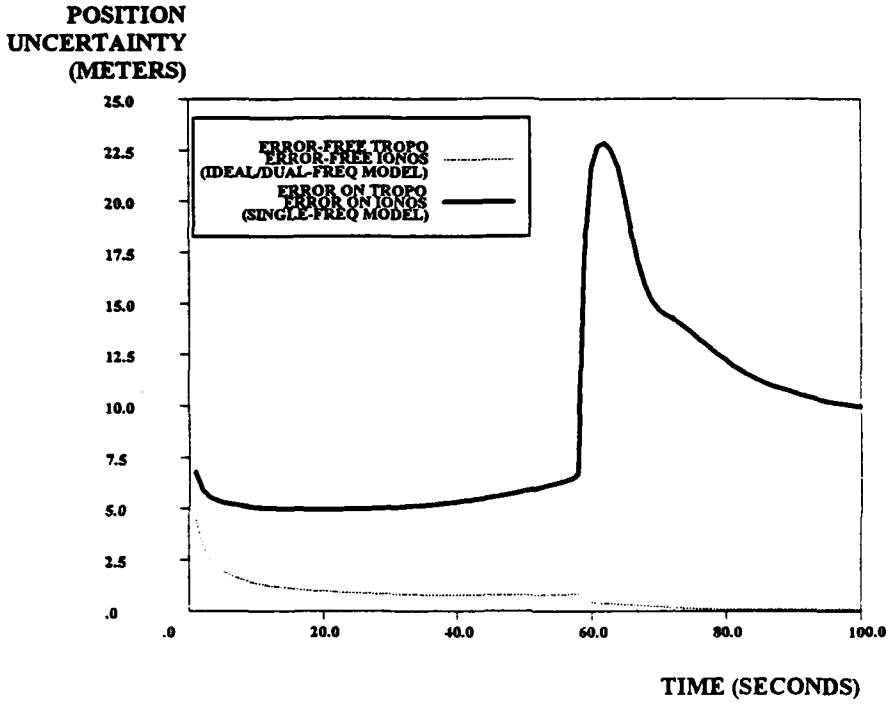

FIGURE 21

UNCERTAINTY USING PSEUDO AND PHASE RANGES

Ideal Case vs. Real-World Case

Single- and Dual-Frequency Models

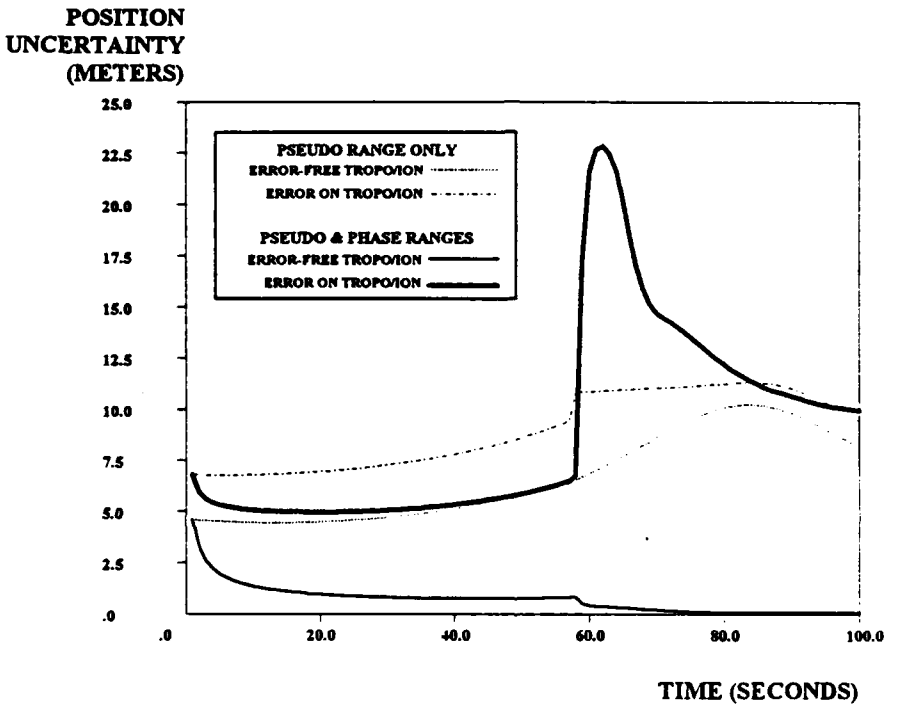

FIGURE 22

COMPARISON OF UNCERTAINTY

USING PSEUDO AND PHASE RANGE COMBINATIONS

w/ and w/o Tropospheric and Ionospheric Errors

Ideal Case vs. Real-World Case

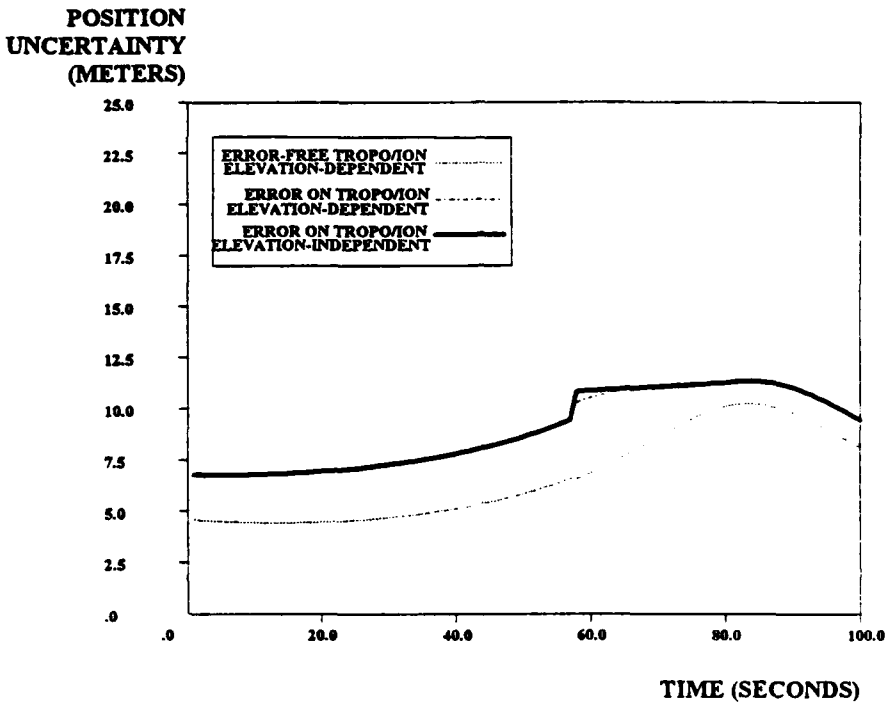

FIGURE 23

UNCERTAINTY USING PSEUDO RANGES

Msmt Model w/ and w/o Elevation-Dependency

Based on Troposphere

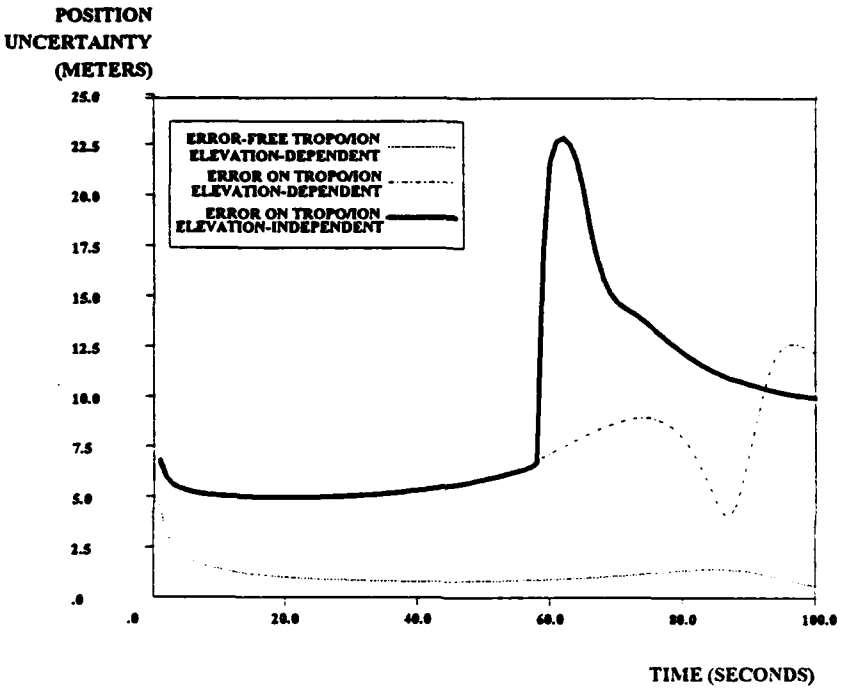

FIGURE 24

UNCERTAINTY USING PSEUDO AND PHASE RANGES

Msmt Model w/ and w/o Elevation-Dependency

Based on Troposphere

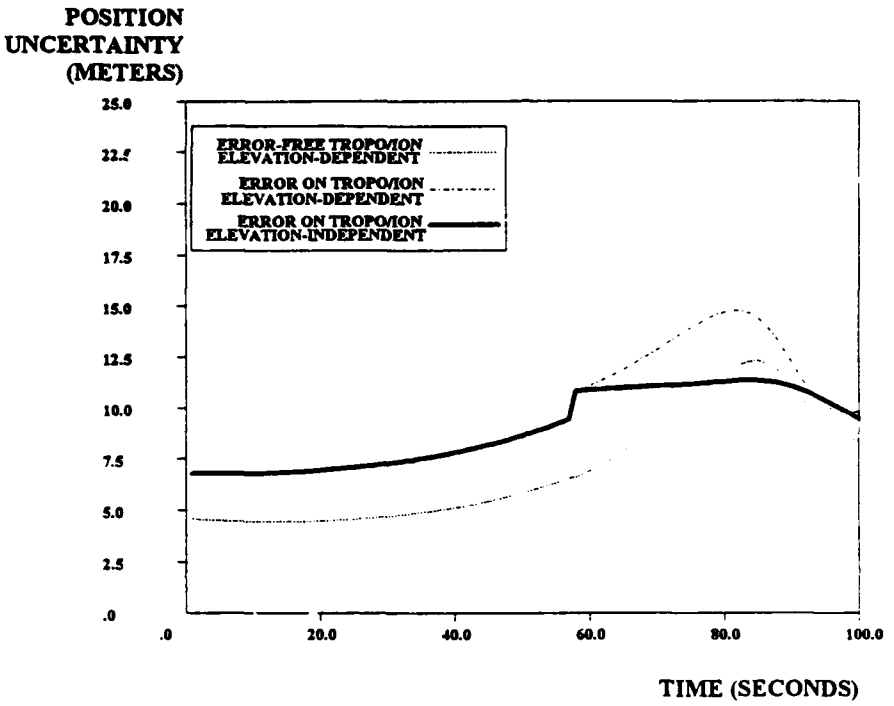

FIGURE 25

UNCERTAINTY USING PSEUDO RANGES

Msmt Model w/ and w/o Elevation-Dependency

Based on Ionosphere

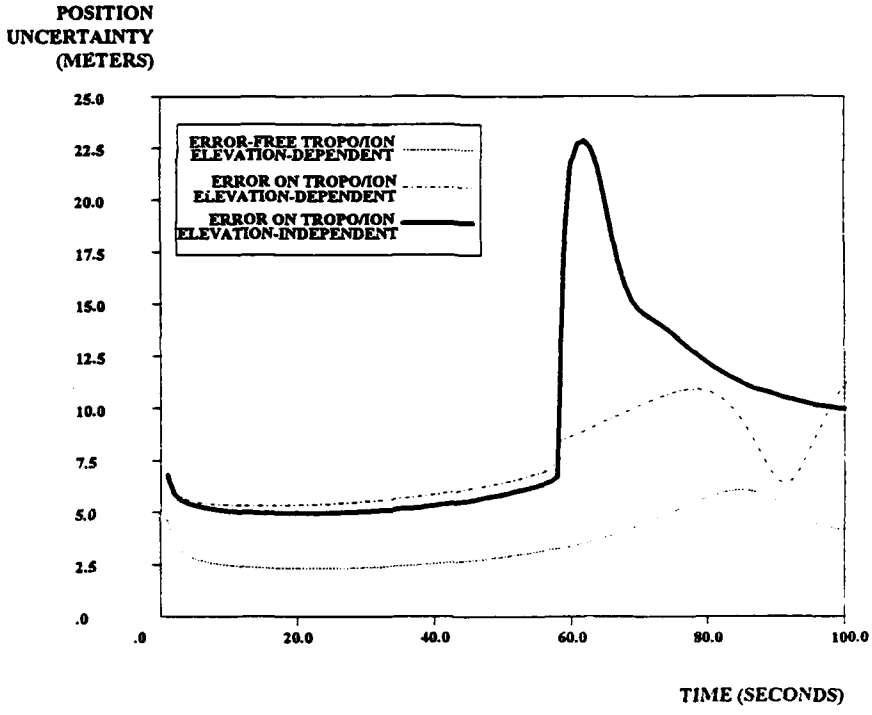

FIGURE 26

UNCERTAINTY USING PSEUDO AND PHASE RANGES

Msmt Model w/ and w/o Elevation-Dependency

Based on Ionosphere

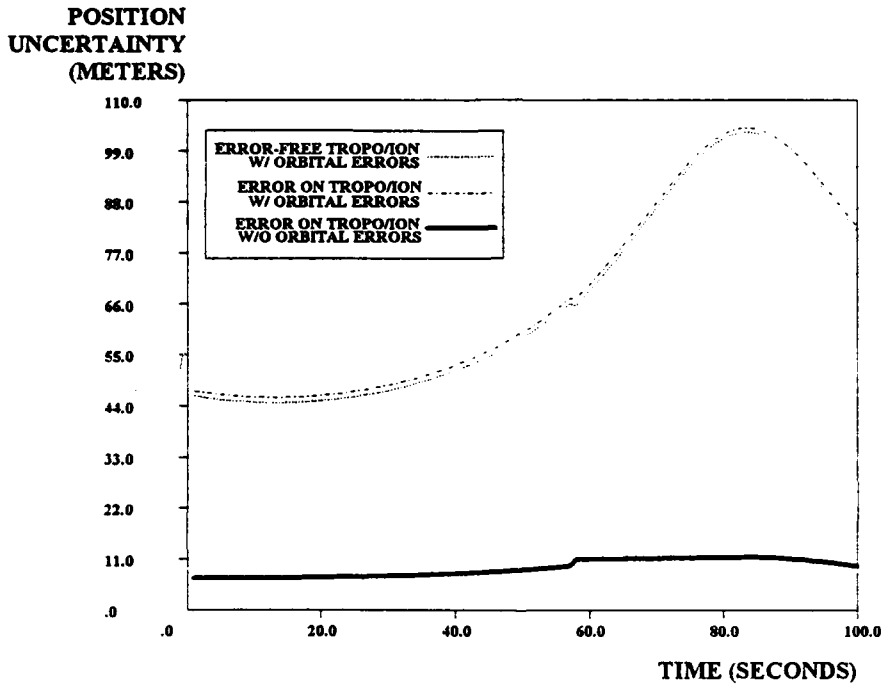

FIGURE 27

UNCERTAINTY USING PSEUDO RANGES

Msmt Model w/ and w/o Radial Orbit Errors

Coefficient Error = 10 meters

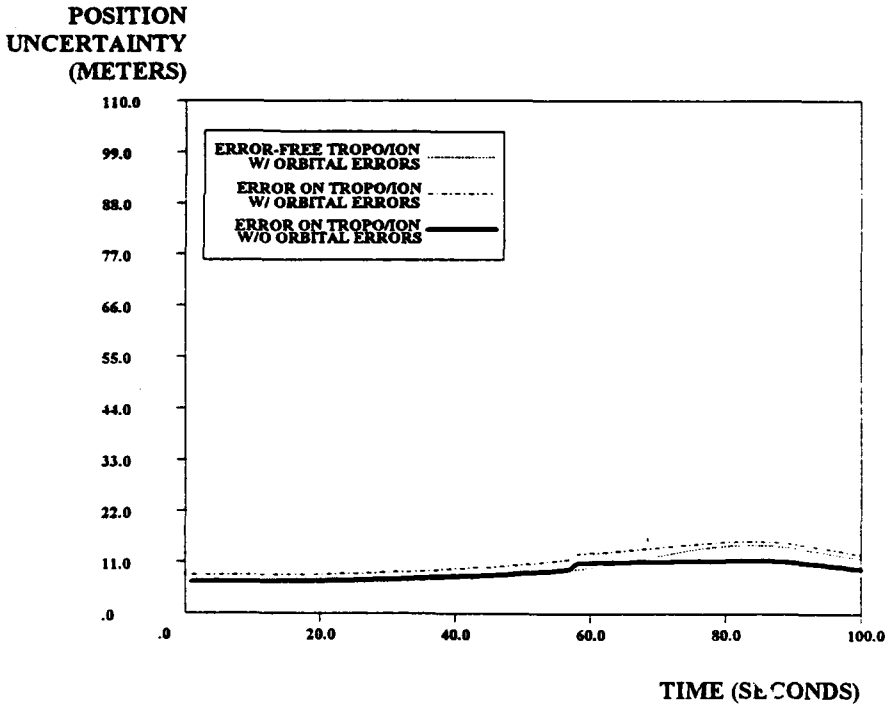

FIGURE 28

UNCERTAINTY USING PSEUDO RANGES

Msmt Model w/ and w/o Radial Orbit Errors

Coefficient Error = 1 meter

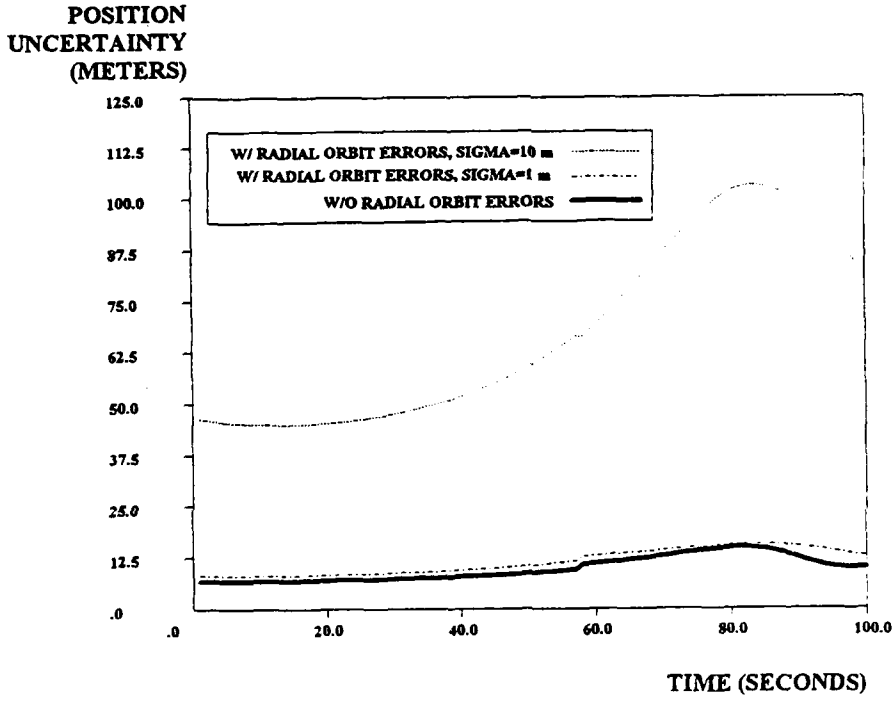

FIGURE 29

UNCERTAINTY USING PSEUDO RANGES

w/ Elevation-Dependency Based on Ionosphere

w/ Tropospheric and Ionospheric Errors

Msmt Model w/ and w/o Radial Orbit Errors

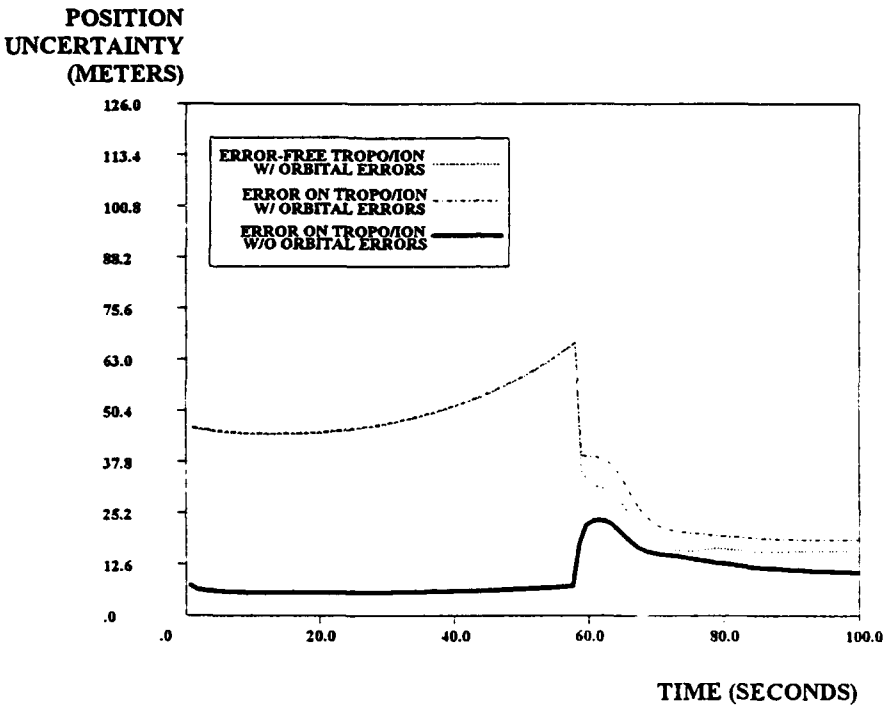

FIGURE 30

UNCERTAINTY USING PSEUDO AND PHASE RANGES

Msmt Model w/ and w/o Radial Orbit Errors

Coefficient Error = 10 meters

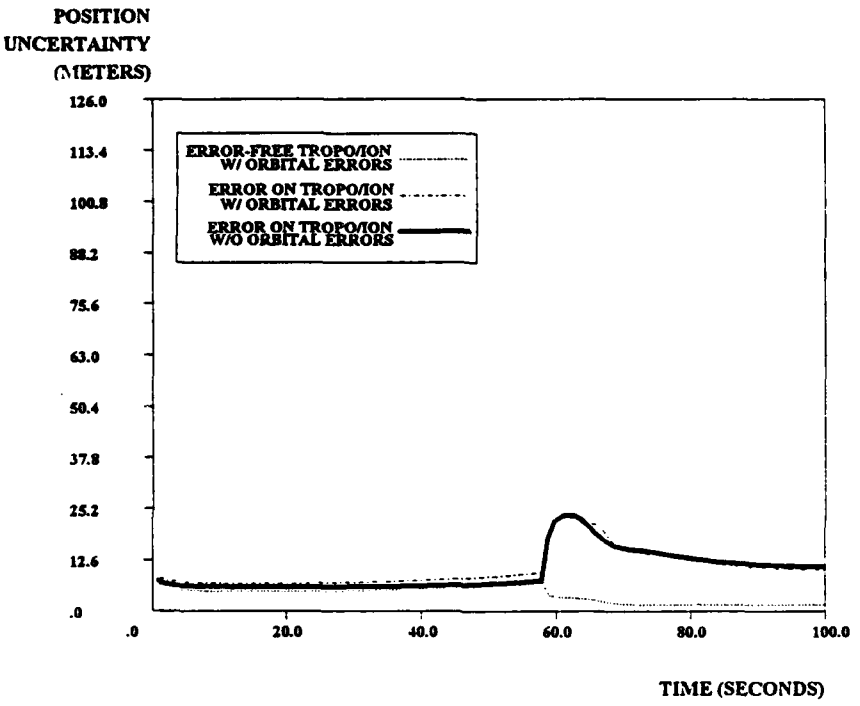

FIGURE 31

UNCERTAINTY USING PSEUDO AND PHASE RANGES

Msmt Model w/ and w/o Radial Orbit Errors

Coefficient Error = 1 meter

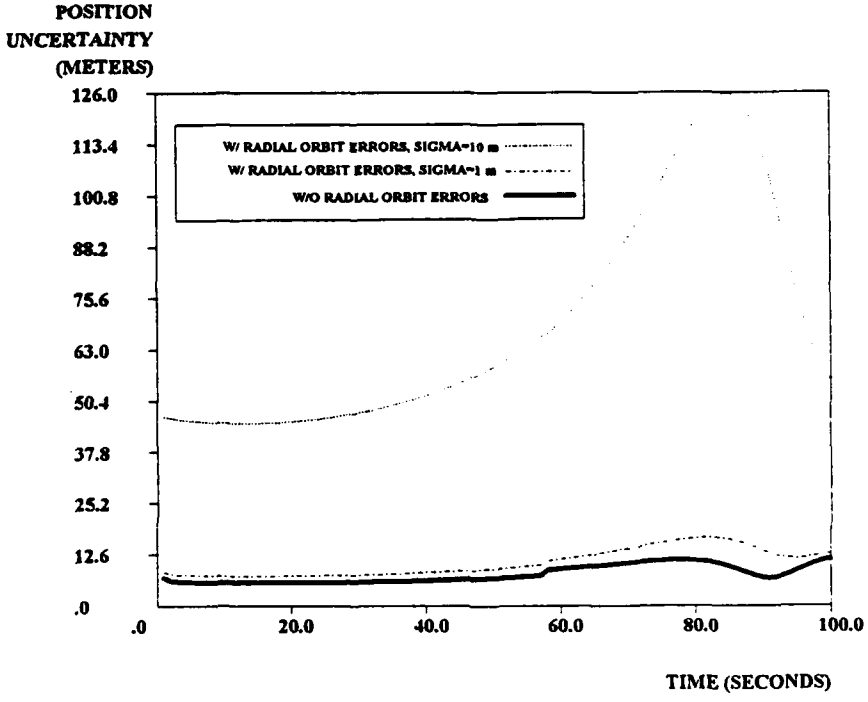

FIGURE 32

UNCERTAINTY USING PSEUDO AND PHASE RANGES

w/ Elevation-Dependency Based on Ionosphere

w/ Tropospheric and Ionospheric Errors

Msmt Model w/ and w/o Radial Orbit Errors

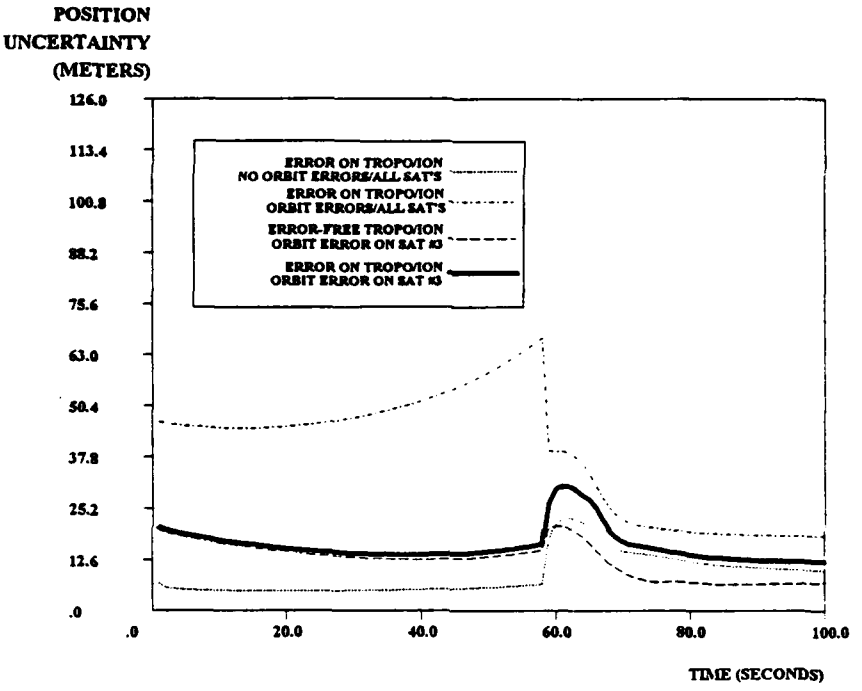

FIGURE 33

UNCERTAINTY USING PSEUDO AND PHASE RANGES

Contribution of a Single Satellite's Radial Orbit Errors

w/ and w/o Tropospheric and Ionospheric Errors

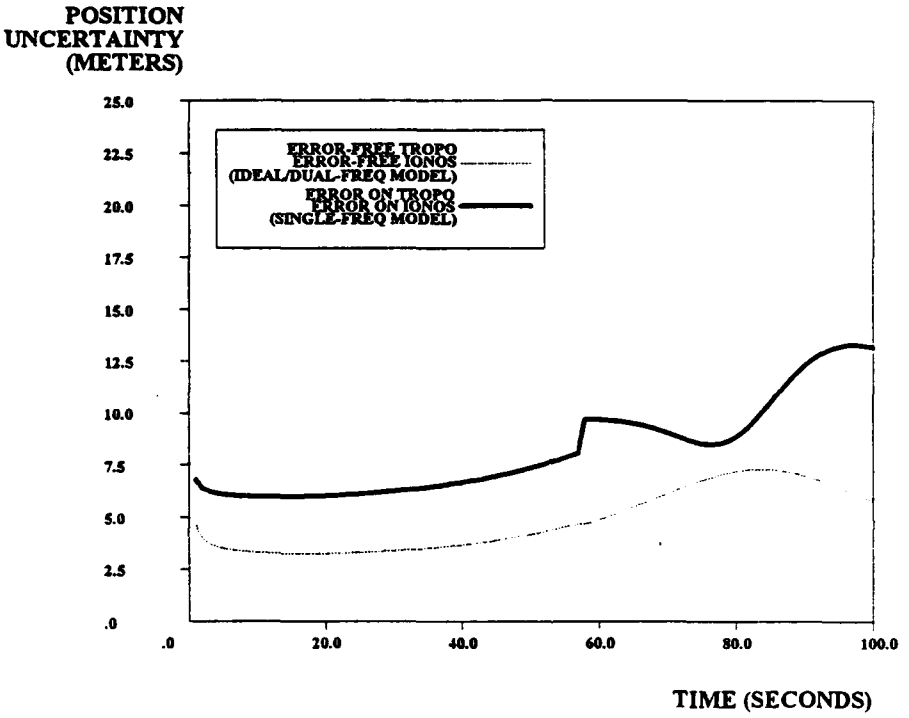

FIGURE 34

UNCERTAINTY USING PSEUDO AND PHASE RANGES

Ideal Case vs. Real-World Noises

Msmt Noise(range) = Msmt Noise(phase)

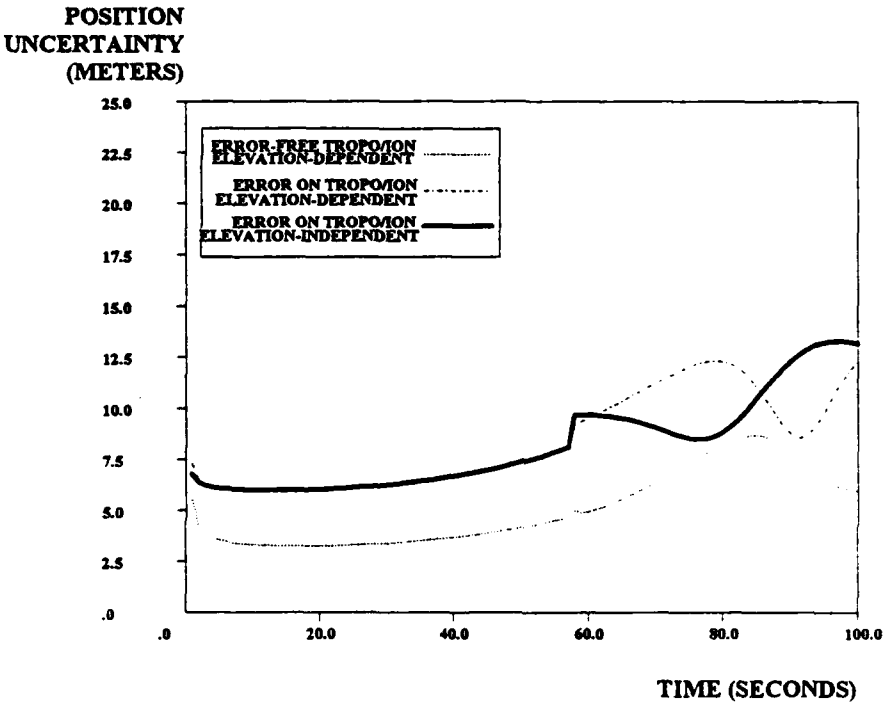

FIGURE 35

UNCERTAINTY USING PSEUDO AND PHASE RANGES

Msmt Model w/ and w/o Elevation-Dependency

Based on Ionosphere

Msmt Noise(range) = Msmt Noise(phase)

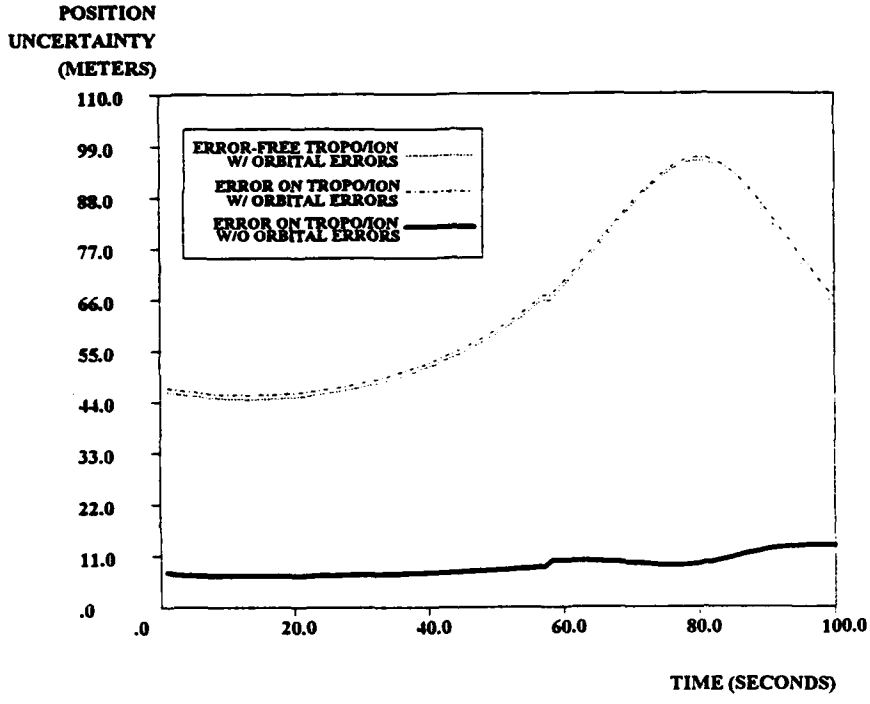

FIGURE 36

UNCERTAINTY USING PSEUDO AND PHASE RANGES

Msmt Model w/ and w/o Radial Orbit Errors

Coefficient Error = 10 meters

Msmt Noise(range) = Msmt Noise(phase)

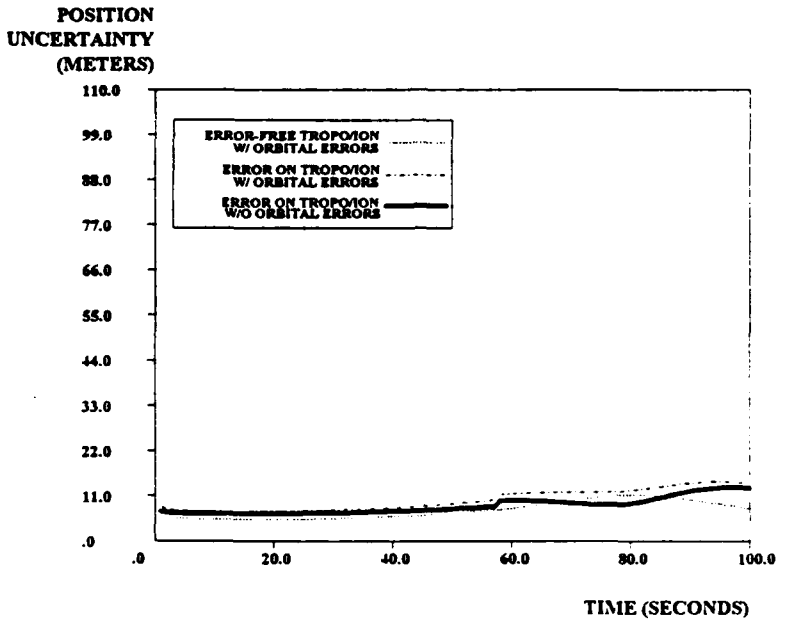

FIGURE 37

UNCERTAINTY USING PSEUDO AND PHASE RANGES

Msmt Model w/ and w/o Radial Orbit Errors

Coefficient Error = 1 meter

Msmt Noise(range) = Msmt Noise(phase)

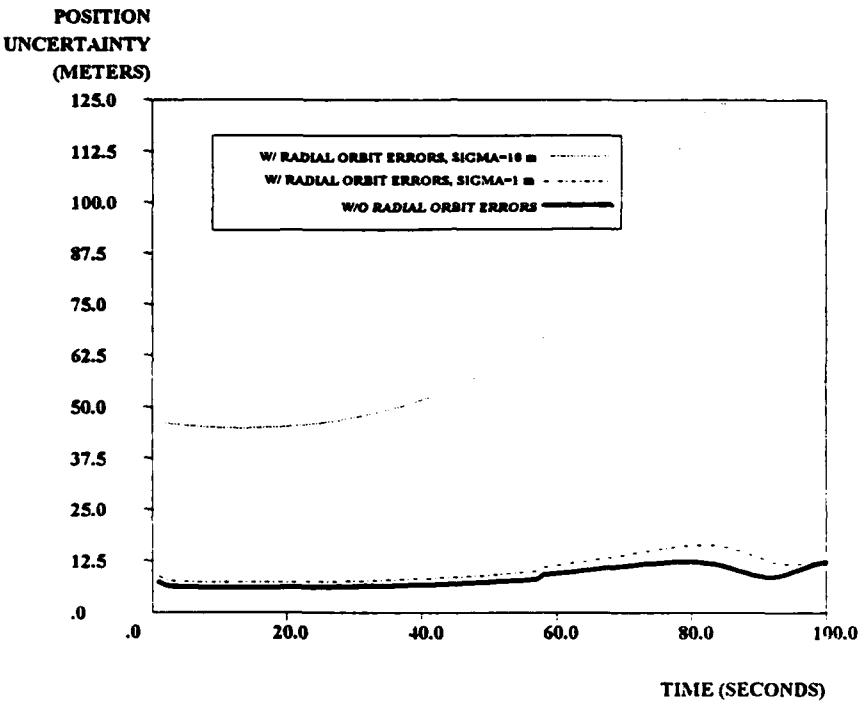

FIGURE 38

UNCERTAINTY USING PSEUDO AND PHASE RANGES

w/ Elevation-Dependency Based on Ionosphere

w/ Tropospheric and Ionospheric Errors

Msmt Model w/ and w/o Radial Orbit Errors

Msmt Noise(range) = Msmt Noise(phase)

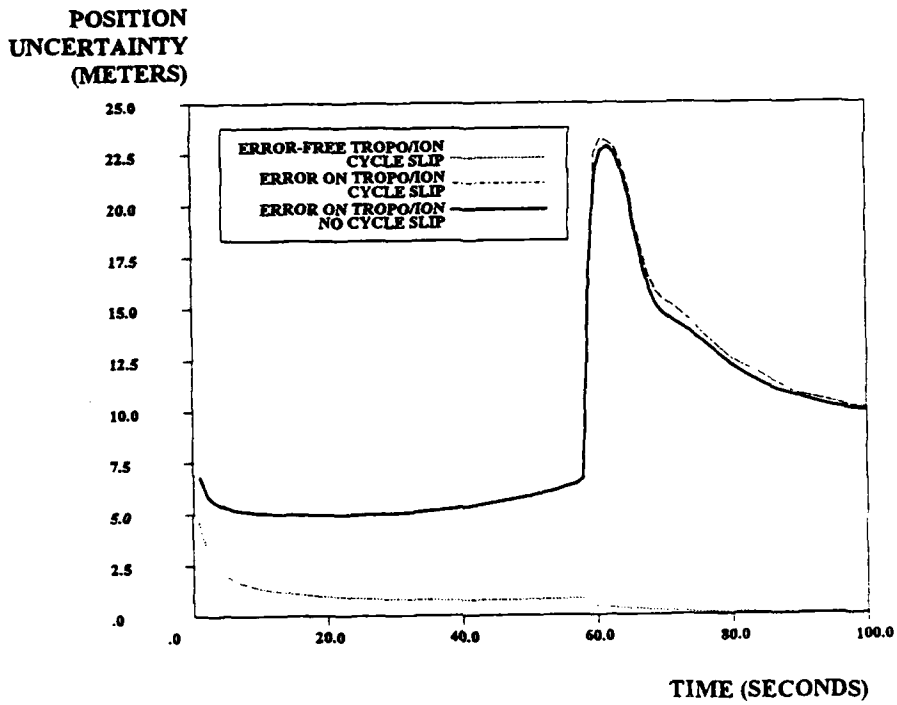

FIGURE 39

UNCERTAINTY USING PSEUDO AND PHASE RANGES

w/ and w/o Tropospheric and Ionospheric Errors

Cycle Slip on Satellite #3 at t=3, t=20, & t=70

CHAPTER V
CONCLUSIONS

5.1 Overview

This thesis examined the uses of different types of GPS data together with different types of biases. The primary theme was to investigate the incorporation of phase range measurements into pseudorange measurements with the use of the MSOFE software package. Iterations of the program were made using combinations of a variety of bias sources (integer ambiguity, tropospheric delay, ionospheric delay, orbital biases, and cycle slips) and different miscellaneous models (equal measurement weightings, elevation-dependent measurement noise models). This chapter outlines the findings of this research. Areas for future research will also be addressed.

In this research, the simulation scenario for data generation utilized a specific broadcast ephemeris, station location, and satellite track. Exact results will be impossible to duplicate under *different* satellite/station geometries, elevations, and ephemeris information. The findings in this research indicate the effects of the different combinations of influences and may be used to surmise the effects on scenarios other than the one used here.

5.2 Summary of Results

By examining the results of the research, one important conclusion is clear: the incorporation of phase range data (known to a millimeter) along with the meter-level pseudorange measurement data vastly improved the overall knowledge of the recovered position of the receiver. With the addition of the phase range measurement, the uncertainty of the position decreased (per epoch) on the order of $1/\sqrt{n}$, where n is the number of measurements.

The addition of unmodeled biases in the "filter" model affects one's ability to recover the station's position. In all cases, the bias-laden models generated a position uncertainty greater than the ideal case with no biases present. Biases in the troposphere did not increase the uncertainty level over the ideal case by as great a magnitude as the ionospheric bias did, because the tropospheric delay was known to 98% and the ionospheric delay only to 50%.

The elevation-dependent model, based on the troposphere, showed little change in the uncertainty when only pseudoranges were used. The (troposphere) elevation-dependent model did, however, indicate an improvement over the elevation-independent model for the pseudo/phase range combinations. The large rise in position uncertainty in the latter model due to the redundant satellite was absent in the former model, due to the adequate weighting of the low (in elevation) satellites. For the ionosphere elevation-dependent model, the pseudorange-only

measurement model did not see improvement due to the redundant satellite. The uncertainty actually rose due to the trade-off between the weighting of the low satellites and the unfavorable geometry caused by essentially omitting the fifth measurement. The pseudo/phase range combination, again, showed an improvement over both the pseudorange-only model and the pseudo/phase range model without the elevation-dependency. However, the degrading geometry due to omitting the redundant satellite could cause a problem in the position recovery.

The presence of the orbital biases served to increase the uncertainty in both measurement models. The greater the *a priori* uncertainty in the orbital bias coefficients, the greater the uncertainty in the receiver's position. As the *a priori* uncertainty of the bias increased to ± 1 m, the overall uncertainty curve from the filter approached that of the single-frequency model which was void of orbital biases.

When the measurement noises of the pseudoranges and phase ranges were equal, the station's position uncertainty for the five-satellite epochs was improved over the unequal-noise case (with presence of no other biases). However, as the geometry degraded due to the movement of the satellites, the equal-noise case could not recover the position to an uncertainty as good as the unequal-noise case. The latter case, using the phase ranges good to ± 1 mm, produced better results in epochs with poor satellite/station geometries.

When orbital errors were incorporated into the equal-measurement-noise model, the uncertainty curves resembled those of pseudorange-only models. The worst uncertainty of all was discovered in the single-frequency, equal-measurement-noise, elevation-dependent (based on ionosphere) case. The uncertainty approached 126 m at its peak and showed no signs of improvement as the redundant satellite came into view.

Overall, the incorporation of mm-level phase range measurements into the m-level pseudorange measurements served to reduce the uncertainty in solving for the unknown variables in the state vector. As more corruption was introduced into the measurement model, the ability to recover accurately the receiver's position was degraded. Often, the elevation-dependent measurement noise model further reduced the uncertainty of the station position, providing that the satellite/station geometry created from omitting a measurement was sufficient enough for adequate recovery. Certainly a trade-off exists in reducing the weighting of a measurement if the geometry of the remaining satellites cannot support the rest of the system. This research set the elevation cut-off at the horizon (0 degrees). Better results could be achieved if the cut-off were raised to a greater level, e.g., 15 degrees. The ionospheric and tropospheric delays at 0 degrees were often prohibitive in one's ability to recover positions to an adequate level.

5.3 Areas for Future Research

This thesis concentrated on the single-frequency GPS receiver to model the measurements. The dual-frequency receiver may serve to provide better results. In the dual-frequency receiver, biases such as the ionosphere (with a $\pm 50\%$ uncertainty) could be eliminated from the problem altogether by combining in a particular way the two measurements at the respective frequencies. This combination, however, has the drawback of amplifying measurement noise. The resulting noise value is *scaled up* by approximately 3 times the original L_1 or L_2 noise value[1]. The trade-off may well be worth the added noise, because the ionospheric delay is very difficult to model, and all attempts to model the ionospheric effects will probably result in errors very much greater than a three-fold increase in measurement noise.

Further research in this area also could include the incorporation of Doppler measurements (time rate of change of phase (ranges)) into the filter process augmenting the pseudoranges and phase ranges. As seen in this research, the inclusion of better-known information serves well to increase the accuracy of the recovered information. An added plus to including Doppler measurements is that there are no integer ambiguity problems to contend with. A trade-off must occur,

---

[1]The noise on the L_1 carrier is amplified by 2.5 times, and the noise on the L_2 is amplified by 1.5 times. The overall effect on the standard deviation, σ, is

$$\sigma^* = \sigma_{msmt}\sqrt{1.5^2 + 2.5^2} = 2.91\sigma_{msmt}.$$

however. Using Doppler measurements, one must attempt to solve for the rate of change of clock drift (i.e., another unknown must be added to the state vector to account for the clock). One might "solve" this situation by increasing the precision of the clock to, perhaps, that of a rubidium clock, known to 1 part in 10^{12}. This way, the unknown frequency drift of the clocks could be "controlled" and act as a stabilizing influence in recovering the position of the receiver.

One final issue must be addressed--the issue of an updated Kalman gain matrix for the augmented, "real-world" situation. Recall from Chapter 2 that, with and without the presence of real-world errors, the covariance update equations take on different forms (see Equations 2-45 and 2-39, respectively). The program MSOFE, however, did not update the Kalman gain matrix (Equation 2-40) to account for the additional vector of errors. In all cases, the Kalman gain used by MSOFE in the update process was the usual filter gain, shown in Equation 4-11.

$$K = P^{-}(H^{-})^{T}[H^{-}P^{-}(H^{-})^{T} + R]^{-1} \tag{5-1}$$

However, this value did not take into account any of the additional real-world error states. Solving for the Kalman gain matrix based on *augmented* predicted residual variances, one gets

$$K_{augmented} = P^{-}(H^{-})^{T}[H^{-}P^{-}(H^{-})^{T} + R + MP_{\gamma}M^{T}]^{-1} \tag{5-2}$$

which incorporates the covariance of the error states into the update process.

Further study should examine the accuracy of the results using MSOFE together with this augmented gain matrix. In MSOFE, the Kalman gain matrix in Equation 4-11 was employed. The **R** matrix was a diagonal matrix due to the lack of correlation of noise between states. By adding the vector of "real-world" errors, $\underline{\gamma}$, to the system, one gets an *augmented* measurement noise, seen in Equation 4-13.

$$R_{augmented} = R + MP_{\gamma}M^{T} \tag{5-3}$$

This matrix is clearly no longer diagonal. Here, the noise becomes correlated between states--a condition ignored by MSOFE, which assumed the same systematic effects for all states. If the same systematic effects did occur epoch after epoch, one could investigate including these $\underline{\gamma}$ states in the "filter" model to attempt to balance the "system" and "filter" models properly in order to gain better information about them. Although MSOFE's methods were satisfactory for investigating the topics in this thesis, they were by no means optimum.

The issue of the P_{γ} matrix should also be addressed. In Chapter 2, we assumed that this covariance matrix remained bounded. However, one should not ignore the situation where some states in P_{γ} become unbounded. As mentioned above, one may desire to treat some states in the $\underline{\gamma}$ vector as unknowns and attempt to solve for them[2]. This situation may set up a condition whereby the covariance values increase rapidly (i.e., $P_{\gamma} \rightarrow \infty$). In this case, the augmented **R** matrix from

[2] Techniques concerning the elimination of parameters may be found in the work by Prijatna, 1992.

Equation 5-3 will also become unbounded (for those states), and the Kalman gain matrix will approach zero (for those states). One cannot easily predict the exact effect on **R** and **K** that an unbounded covariance matrix will have; one may or may not be able to solve for the desired states in the $\underline{\gamma}$ vector. Further, if the gain matrix approaches zero, then the states will not be updated from the current states (i.e., one would not see a reduction in **P** from P^- to P^+). Further research in this area could investigate the effect of this situation on the outcome of the uncertainty of the unknowns and determine if this situation is detrimental to the adjustment procedure and the recovery of accurate information.

LIST OF REFERENCES

1. Brown, Robert Grover, *Introduction to Random Signal Analysis and Kalman Filtering*, John Wiley & Sons, 1983.

2. Carlson, Neal A., and Musick, Stanton H., *Users' Manual for a Multimode Simulation for Optimal Filter Evaluation (MSOFE)*, AFWAL-TR-88-1138, Wright-Patterson AFB OH: Avionics Lab, AFWAL/AARN-2, April 1990.

3. Gelb, Arthur (editor), *Applied Optimal Estimation*, The Analytic Sciences Corporation, The M.I.T. Press, 12th ed., 1992.

4. Goad, Clyde C., *Optimal Filtering of Pseudoranges and Phases from Single-Frequency GPS Receivers*, NAVIGATION: Journal of the Institute of Navigation, Vol. 37, No. 3, Fall 1990, pp. 249-262.

5. Goad, Clyde C., and Goodman, L., *A Modified Hopfield Tropospheric Refraction Correction Model*, presented at the Fall Annual Meeting, American Geophysical Union, San Francisco, CA, 12-17 December 1974.

6. Leick, Alfred, *GPS Satellite Surveying*, John Wiley & Sons, 1990.

7. Maybeck, Peter S., *Stochastic Models, Estimation, and Control*, Volume 1, San Diego, CA, Academic Press, 1979.

8. Musick, Stanton H., *SOFE: A Generalized Digital Simulation for Optimal Filter Evaluation User's Manual*, Air Force Avionics Laboratory, Wright-Patterson Air Force Base, Ohio, June 1978.

9. Prijatna, Kosasih, *Alternative Models To Derive Ionospheric Parameters from GPS Dual-Band Observations*, Thesis, The Ohio State University, 1992.

10. Spilker, J.J., Jr., *GPS Signal Structure and Performance Characteristics*, Papers Published in NAVIGATION: Journal of the Institute of Navigation, Vol. 1, 1980.

11. Stacey, Richard D., *A Navigation Reference System (NRS) Using Global Positioning System (GPS) and Transponder Aiding*, Thesis, AFIT/GE/ENG/91M-04, 6 March 1991.

12. Wells, David (editor), *Guide to GPS Positioning*, Canadian GPS Associates, 1987.